ULTRA HIGH DATA-RATE OPTICAL TRANSMISSION NETWORKS

Part 1: Design of an optical system testbed for ultra high speed long haul transmission

Part 2: Analysis and Reduction of Polarization Dependent Penalty in Phase Shift Keying

Demodulators

By

Dragos Cotruta

Electrical Engineering

McGill University, Montreal

August, 2010

A thesis submitted to McGill University

In partial fulfillment of the requirements of the degree

Of

Master in Electrical Engineering

Abstract

The thesis consists of two different topics: In part 1, the design of an optical system testbed for long haul transmission using a re-circulating loop, is presented. The testbed operates at 40 Gb/s, it simulates an 1800 km link, with optical amplifiers every 80 km, and 16-32 DWDM channels. The theoretical elements involved in the testbed design are reviewed. The optical components are described and selected. The optical system design parameters are presented as well as design targets and optimization parameters. The final implementation is presented and propagation simulations are performed with RZ/NRZ DPSK, QPSK modulation formats to demonstrate the testbed functionality. In part 2 of the thesis, The BER penalty due to PDf in a DPSK demodulator is analyzed and its effect mitigated. A readily available technique is developed that allows measuring the individual contributions of PDf and PDL on BER and calibrate the demodulator in order to reduce the effective PDf by a factor of two which represents an almost 40% reduction in BER penalty due to PDf. The BER penalty due to PDf is measured for 10- vs. 40-GHz, RZ vs. NRZ DPSK demodulators. Finally, PDf mitigation is demonstrated using a PDL emulator, allowing a 75% reduction in polarization sensitivity.

Résumé

La thèse se compose de deux sujets différents: Dans la partie 1, la conception d'un banc d'essai pour simuler un système optique pour la transmission longue distance à l'aide d'une boucle de recirculation, est présentée. Le banc d'essai fonctionne à 40 Gb/s, il simule un lien de 1800 km, avec des amplificateurs optiques à tous les 80km, et 16-32 canaux DWDM. Les éléments théoriques impliqués dans la conception du banc d'essai sont passés en revue. Les composantes optiques sont décrites et sélectionnées. Les paramètres de conception de systèmes optiques sont présentés ainsi que des objectifs de conception et d'optimisation. La mise en œuvre finale est présentée et des simulations de propagation sont réalisées avec les formats de modulation OOK, DPSK, QPSK RZ / NRZ pour démontrer la fonctionnalité du banc d'essai. Dans la partie 2 de la thèse, la pénalité due au PDf dans un démodulateur DPSK est analysée et ses effets réduits. Une technique facilement disponible est développée qui permet de mesurer les contributions individuelles du PDf et PDL sur le BER et de calibrer le démodulateur afin de réduire par un facteur de deux le PDf effectif, ce qui représente une réduction de près de 40% de la pénalité due au PDf sur le BER. La pénalité due au PDf sur le BER est mesurée pour les 10 - 40-GHz vs RZ NRZ dans les démodulateurs DPSK. Enfin, la réduction de la pénalité due au PDF est démontrée en utilisant un émulateur de PDL, ce qui permet une réduction de 75% de la sensibilité à la polarisation.

Acknowledgements

First and foremost, I would like to thank my supervisor, Prof. David V. Plant, who has supported me throughout the thesis with his patience and knowledge whilst allowing me to work in my own way. Professor Plant has both broadened and deepened my knowledge and insight in the subject matter, by opening my eyes to a multitude of different perspectives on all the topics covered in the thesis and beyond. Also, Professor Plant helped me on many other levels: he shared with me his knowledge from different fields related to engineering, he gave me engineering carrier advice, and he helped me with personal issues, making him the best supervisor and professor.

Next, I would like to thank my co-supervisor, Prof. Odile Liboiron-Ladouceur, for her advice, supervision, and contribution, which made her a key person of this research and so to this thesis. I would also like to thank her for her endless determination and patience correcting the multiple drafts of my work. Without her valuable input, I would have not achieved a high degree of quality throughout my thesis work.

I would also like to thank Prof. Lawrence Chen, Martin Rochette and Andrew Kirk for their tutoring skills and generosity. They opened the world of photonics and inspired me as research role models.

I want to thank Xian Xu for helping me throughout my experimental work in the lab. You have been a great lab partner that stimulated a lot of interesting talks. Without your presence, the long nights spent in the lab would seem never ending. I also want to thank Pegah Seddighian for helping me in the lab with your extensive experience as an experimentalist and technical knowledge. I want to express my appreciation to all my colleagues that helped me throughout the completion of my thesis: Raja Ahmad, for your help characterizing the Optilab's EDFAs; Mahammad Pasandi, for your very interesting conversations; Zaobing Tian, for opening the Chinese culture to me; Alex Zang, for your entertaining nature. I want to express my gratitude toward: Joshua Schwartz, our lab manager that more than once took time to help me find those misplaced equipments; Carrie Serban, Kay Johnson and Christopher Rolston for their valuable time and help for all the administrative activities.

I want to express my special thanks to my friends, Matei Mireuta and Payman Samadi, for their support and friendship all these years. They are and will continue to be an important part of my life.

Finally, I want to thank my parents Gabriela and Teodor Cotruta for their endless love, support and sacrifices over all these years. Without them, I would have not got to where I am today, placing them at the root of all my achievements and making them the most important persons in my life.

Table of Contents

Tabl	e of Cor	ntents .		6	
Tabl	e of Fig	ures		10	
Intro	duction			12	
1 Design of an optical system testbed for ultra high speed long haul transm					
1.	.1 B	ackgro	ound Theoretical Review	19	
	1.1.1	Modu	llation Formats	19	
	1.1.	1.1	ASK Modulation format	20	
	1.1.	1.2	PSK Modulation format	21	
	1.1.	1.3	FSK Modulation format	23	
	1.1.	1.4	Data formats	23	
	1.1.	1.5	Non-Return to Zero	23	
	1.1.	1.6	Return to Zero	24	
	1.1.	1.7	Optical Signal	24	
	1.1.	1.8	Optical signal generation	25	
	1.1.	1.9	Optical signal recovery	30	
1.	.2 C	ptical I	Link Components	32	
	1.2.1	Trans	smitter	32	
	1.2.	1.1	Laser	32	
	1.2.	1.2	Modulator	33	
	1.2.	1.3	Booster EDFA	34	
	1.2.2	Trans	smission link	35	
	1.2.2	2.1	Optical Fiber: SMF vs. LEAF	35	
	1.2.2	2.2	Inline EDFA	36	
	1.2.2	2.3	Dispersion Compensation	37	
	1.2.3	Rece	iver	38	
	1.2.3	3.1	Demodulator	38	
1.	.3 C	ptical ⁻	Testbed Design	39	
	1.3.1	Recir	culating loops in literature	39	
	1.3.2	Optic	al recirculating loop proposed design	44	
	1.3.2	2.1	Transmitter	45	
1.3.2.2 1.3.2.3 1.3.2.4		2.2	Transmission Line	47	
		2.3	Receiver	52	
		2.4	Control switches and loop synchronization	53	
	1.3.2	2.5	Power Evolution	54	

1.3.3 Experimental Methodologies	55
1.3.3.1 Recirculating loop power re-calibrati	on55
1.3.3.2 Synchronization of control switches	and error detector56
1.3.3.3 Measuring eye diagrams with a reci	rculating loop57
1.4 Simulation Results	58
1.5 Experimental results and setup improvement	considerations61
1.6 Conclusion	64
1.7 References	66
2 Analysis and Reduction of Polarization Dependent	Penalty in Phase Shift Keying
Demodulators	70
2.1 Background Theoretical Review	70
2.2 PDf Performance Penalty Analysis	72
2.2.1 Measurement Methodology	72
2.2.2 PDf effect versus bit rate	75
2.2.3 PDf versus pulse carving	79
2.3 Mitigating PDf Effect	82
2.3.1 Cost-effective Solution	82
2.3.2 PDL to Compensate PDf	82
2.4 Conclusion	85
Conclusion and Future Work	86
2.5 References	88
Appendix Optical Specs	90
Laser	90
AWG	91
Mach-Zehnder modulator	92
RF amplifier	93
Booster EDFA	94
Inline EDFA	94
Pre-Amplifier EDFA	96
Acousto-Optical Modulator	97
Parameter	97
Specification	97
Unit	97
Acoustic Mode	97
Longitudinal	97
	97

Wavelength Range	97
1300-1600	97
nm	97
Static Transmission	97
>97	97
%	97
Operating Frequency	97
35	97
MHz	97
Diffraction Efficiency	97
>85	97
%	97
Light Polarization	97
Random	97
	97
Optical Power Density	97
<50	97
KW/cm ²	
Acoustic Aperture Size	97
2	
Mm	97
Rise Time	97
260	
ns/mm Beam Diamete	
Deflection Angle@1550nm	
20.6	97
rad	
RF Power Level	
<0.5	
W	97
Impedance	
50	
Ω	97
VSWR@35MHz	97
1.2:1	97
-	97

Optical fibers	98
Dispersion Compensation	99
Demodulator	100
Photodetector	101
Clock Recovery	102

Table of Figures

Figure 1 Modulated optical signal for ASK, PSK and FSK given a input electrical signal at t	he top
[2]	20
Figure 2 Mach-Zehnder Modulator and its transfer function [3]	26
Figure 3 MZ transfer function showing the bias point and operation range of OOK (left), an	d the
corresponding signal constellation (right)	27
Figure 4 MZ transfer function showing the bias point and operation range of BPSK (left), at	nd the
corresponding signal constellation (right)	27
Figure 5 MZ output phase (rad) and normalized output intensity	28
Figure 6 MZ transfer function showing the bias point and operation range of QPSK (left), a	nd the
corresponding signal constellation (right)	29
Figure 7 MZ transfer function showing the bias point when operating as a carver	29
Figure 8 Modulator setups used for generating RZ-DPSK and RZ-DQPSK	30
Figure 9 Distributed feedback, DFB, laser diode [28]	32
Figure 10 Mach-Zehnder Modulator	33
Figure 11 Erbium Doped Fiber Amplifier	34
Figure 12 Different fiber types [30]	36
Figure 13 Dual stage Inline EDFA with mid-stage access [31]	37
Figure 14 Dispersion compensation fiber characteristics	38
Figure 15 FBG dispersion compensation	38
Figure 16: Schematic of the fiber-based DPSK demodulator by ITF Labs/Avensys	39
Figure 17 Reconfigurable recirculating loop transmission setup to enable cascaded 3R	
regeneration with a variable 3R regeneration spacing [32]	40
Figure 18 Experimental setup of the recirculating loop using two 3dB optical switches [33].	41
Figure 19 Recirculating loop setup for single channel 170 Gb/s transmission up to 4000km	[34] 42
Figure 20 Setup of PMD compensation experiment using recirculating fiber loop with loop-	
synchronous polarization scrambling [35]	42
Figure 21 Optical Recirculating Loop using LEAF fiber with pre and post dispersion compe	nsation
	44
Figure 22 Simulation of the dispersion Evolution for two loop trips using only pre and post	
dispersion compensation for two different fiber types, LEAF and SMF	50
Figure 23 Simulation of the dispersion evolution for one full loop using full inline dispersion	i
compensation for two types of fibers, LEAF and SMF	51
Figure 24 Data timing diagram showing the logical signals controlling the recirculating loop	57

Figure 25 Optiwave simulation results. Eye diagram of 16 co-propagating channels at 40Gb/s	
after 600km transmission, 50GHz channel spacing, DPSK - LEAF fiber (left), SSMF (center),	
SSMF /w inline DCF (right)59	9
Figure 26 Optiwave simulation results. Eye diagram of one of the 16 co-propagating channels at	
40Gb/s after 600km transmission, 50GHz channel spacing, QPSK - LEAF fiber (left), SSMF	
(center), SSMF /w inline DCF (right)60)
Figure 27 Optiwave simulation results. Eye diagram of 16 co-propagating channels at 40Gb/s	
after 1800km transmission, 100GHz channel spacing, DPSK - LEAF fiber (left), SSMF (center),	
SSMF /w inline DCF (right)6	1
Figure 28 Gain flatness of Optilab's inline EDFAs: input signals of -15.7dBm total power (left),	
output signals of 10.1dBm (right)63	3
Figure 29: Schematic of the fiber-based DPSK demodulator by ITF Labs/Avensys7	1
Figure 30 The Poincare Sphere showing the 14 SOP that were chosen for these experiments [12]	-
Figure 31: Power penalty versus frequency shift for two orthogonal SOPs of a 10-Gb/s	
demodulator74	1
Figure 32: Signal spectra of the demodulator showing both the destructive and constructive ports.	,
with (top) a zoom on a spectral null of the destructive port and (bottom) of the constructive port.75	5
Figure 33: Comparison of the spectrum of a 10-GHz and a 40-GHz DI77	7
Figure 34: Experimental setup for PDf analysis versus data rate	7
Figure 35: BER versus frequency detuning. (a) All measurements shown. (b) zoom in dotted	
rectangle PDf and penalty for the respective DIs78	3
Figure 36: (a) Spectra of 40-Gb/s NRZ- and RZ-DPSK signals (b) showing the effect of frequency	,
offset	9
Figure 37: Spectral profile of a RZ-DPSK signal80)
Figure 38: BER versus frequency detuning for demodulated 40 Gb/s RZ- and NRZ- DPSK signals	s:
a) all measurements, b) zoom closer to transmissivity peak8	1
Figure 39: (a) BER penalty vs. frequency shift of the slow (red dots) and fast (blue dots)	
polarization axis of a 10 Gb/s demodulator. (b) Reduced PDf with calibration. (The continuous	
lines in graphs above represent the fitted curves to the dot experimental data on the same graph)	ļ
8	1
Figure 40: PDf mitigation with BER high and BER low representing the highest and lowest	
measured BER, respectively, for ten measurements83	3
Figure 41 O-factor penalty due to PDI	4

Introduction

The aim of any communication system is to transfer a lot of information quickly and with no errors. Whether it's data, voice or video, or whether it's carrier, enterprise or residential, the difference in requirements can be summarized in terms of how much (data rate and its limit capacity) and how many errors; and lately how fast (latency) [6]. Since the inception of telecommunications at the beginning of the 20th century, engineers have been faced with 2 goals: improving each of these aspects separately and solving the aforementioned tradeoff at a given technological stage [1]. The growing demand for any of these aspects is easy to understand: sharing information, watching the latest high definition movies, playing high definition games, getting the stock market data fractions of a second before the competitor and transferring millions in offshore bank accounts without losing any of the leading digits.

Optical communication is the same as other wave communications (radio, micro-wave) in the sense that it uses electromagnetic carrier waves to carry information [1]. As the usable (low impairments) electromagnetic spectrum is limited for a certain type of wave communication, the frequency bandwidth becomes an expensive currency required to generate a signal of a certain capacity [2].

Whereas the carrier is always an analogue wave, the information can be either analog or digital in terms of whether the signal is composed of discrete or continuous values. Discrete values imply steeper transitions (i.e. more bandwidth) but are well defined. Analogue signals require less bandwidth but are also less well defined, hence more error prone [1].

The first radio frequency communication systems were commercially deployed in 1920s, having carrier frequencies of ~10 KHz. In the 1950s, microwave frequency communication systems started being deployed, with ~1GHz carrier frequencies, and consequently more capacity. With ~100 THz carrier frequency, the first optical

communication systems were commercially deployed in the 1980s, bringing about much higher capacity and arguably the information age. Since the 1980s, optical data rates increased from ~45Mb/s to >1Tb/s with latest 40Gb/s/channel technologies, and approaching 10Tb/s with the upcoming 100Gb/s/channel technologies [2].

Initial research in optical communications can be mainly attributed to material science. The optical fiber suffered from high signal attenuation, almost 20dB/km, thus needing regeneration very often and not commercially appealing [4]. The reduction of fiber loss to 0.2dB/km renewed interest in the field and stimulated research, as lasers that can operate in the low loss fiber frequency regime were needed. Still, with long distances to be covered, there was still need of signal regenerators, which required transforming the optical signal to its electrical counterpart and back to optical (OEO conversion). The cost of OEO conversion was still considerable. As such, the development of optical amplifiers that reduced the need of electronic regenerators made a huge leap in the optical communication business case [1].

One characteristic of optical communications is the need of a confined transmission medium (i.e. optical fiber) to keep light from being scattered as it passes through the atmosphere and for avoiding potential obstacles. Given the high cost of deploying optical fiber [2] for 1000s of km of oceanic or continental links, research started focusing on how the same medium (i.e. optical fiber) can be used to carry more data [1]. The answer to this question lies in optical multiplexing.

Time division multiplexing (TDM), combines multiple optical data streams into a single stream, by allocating different time slots to the different optical streams. Even if the speed of electronics can be limited in terms of how fast the bits can be generated, different lower rate optical streams can be interleaved in time to generate a higher rate optical stream. Two of the main reasons we are still operating far below the theoretical capacity of an ideal optical link are fiber dispersion and non-linearities. Fiber dispersion spreads the optical pulse, which overlaps with adjacent pulses making them unreadable.

Dispersion compensating optical modules were developed to combat chromatic dispersion (section 1.2.2) but other types of dispersion such as polarization mode dispersion were still difficult to solve with optical modules. An example of non-linearity is self-phase modulation (SPM). SPM, like other non-linearities, is due to the refractive index being dependant on optical power and becomes substantial at high optical powers. The difference in refractive index between the '0' and '1' levels creates a phase difference between them, impairing their correct detection [1].

As the data rates are increased with TDM, the pulses become much shorter making them more sensitive to both dispersion and non-linearities [1].

Wavelength division multiplexing (WDM) and Dense WDM (DWDM) schemes divide the available spectrum into several non overlapping frequency bands. Each band corresponds to a channel with a certain carrier frequency. All channels co-propagate in the optical fiber and optical filters are used to combine or individually access the channels. Although WDM technique covers the whole spectrum, the separation in fixed bands (potential wavelength contention) as well as the inter-channel dead zones, is wasteful of bandwidth [1].

Advances in optical multiplexing schemes can involve optimizing a cost effective hybrid OTDM / WDM solution [1], reduction in WDM wasted bandwidth by using flexible grid optical filters [1] and properly adjusted signal bandwidths to reduce inter-channel dead zones, but huge benefits are not expected [1]. However, most current research focuses on advanced modulation techniques which are tolerant to dispersion and nonlinearities, and allow higher data rates in the currently deployed channels, without prohibitive penalties [1, 2]. Most of the deployed 10Gb/s lightwave systems are using the non return to zero on-off keying (NRZ-OOK) modulation format (see section 1.1.1) [1]. This modulation format is preferred to any other formats as it provides a very cost effective solution to 10 Gb/s long haul optical systems. As the data rates go beyond 10 Gb/s, the penalties from chromatic dispersion (CD), polarization mode dispersion (PMD) and

nonlinear effects, become much greater than in traditional systems [1]. There is need to switch to new modulation formats that are more tolerant to such impairments. One modulation format is the Return to Zero (RZ). As the pulse occupies a fraction of the bit period, it is more tolerant to pulse broadening. Also, for the same average power, we can send signals with higher peak powers, thus improving OSNR. All these benefits come with a price in bandwidth; the RZ format uses twice as much bandwidth as NRZ [1]. Over the last few years, phase shift keying (PSK) attracted more attention compared to amplitude shift keying (ASK) since the amplitude modulation at high optical powers is accompanied by high nonlinearities [1]. Further, to increase spectral efficiency, which is very low in current lightwave systems (0.2bit/s/Hz) [1], we can use modulation formats as Quadrature PSK (QPSK) and Differential QPSK (DQPSK), which use two orthogonal carriers to effectively double the data rate. Furthermore, we can use two orthogonal polarizations to increase even more the spectral efficiency in modulation format as Polarization Multiplexed – QPSK (PM-QPSK) and Polarization Multiplexed – DQPSK (PM-DQPSK). An optical stream that uses PM-(D) QPSK as its modulation format with 50GHz channel spacing has a spectral efficiency of 1.6bit/s/Hz an increase of 8 times the current deployed systems [1].

The hardware needed to exercise the additional degrees of freedom (such as optical hybrids [7]) is not cost prohibitive. The limiting factor is the increased error rate due to closer placed constellation points or, put differently, the price of high performance real-time converters / processing required keeping the performance constant [5]. Indeed, advanced modulation techniques require costly development of digital signal processing (DSP) methods for processing closely spaced symbols, but the real showstopper has traditionally been analog to digital converters (ADC) not being able to operate at increasingly higher data rates. The development of powerful (i.e. up to 10GS/s with 4 symbols) ADC/DAC [5], allowed the deployment of the advanced modulation techniques described above, while simultaneously enabling dispersion compensation to be performed electronically instead of optically. The electronic dispersion compensation

not only provides cost reduction compared to optical dispersion compensation, but also increase flexibility and reach [1].

A complete solution to modern optical systems is an optimization problem of many variables which includes: link budgets, penalties associated to different modulations schemes, algorithms to combat these impairments real time and which can be implemented in hardware in a cost and power consumption effective manner [5].

A research lab's need for an optical system testbed operating at high data rates, allowing testing of new modulation techniques, ensues.

The purpose of Part 1 of the thesis is to build a 40 Gb/s optical system testbed that simulates an ultra-high bit rate long haul transmission. It uses a recirculating loop to reduce the cost compared to the equivalent amount of fiber spans, and supports 16-32 DWDM channels.

Several design iterations, each containing several steps, are involved in the building of an optical system testbed. First, the optical system design specifications need to be derived based on the application. Next the transmitters/receiver pairs are chosen to provide a cost effective solution. Based on the system parameters, the link's various components are chosen to satisfy the previously calculated link budgets. In this report only the final solution is presented.

The next task undertaken in this project was to investigate a penalty incurred by commonly used modulation technique: the modulation is differential phase shift keying (DPSK) and the penalty investigated is polarization dependant frequency shift (PDf).

In the metro networks, differential phase shift keying (DPSK) is arguably becoming a format of choice due to its more relaxed optical signal to noise ratio (OSNR) margin and greater tolerance to nonlinear effects, which are particularly important at higher data rates. Phase shift keying demodulators for direct-detection exhibit a performance

penalty due to their inherent polarization dependence referred as polarization dependent frequency shift (PDf).

A technique is first developed to accurately measure the PDf-induced penalty and distinguish it from other polarization based impairments such as polarization dependent loss (PDL). The PDf-induced penalty is shown to decrease with data rates even for larger PDf values. The analysis explains why the PDf ratio, defined as PDf over the free spectral range (FSR), better determines the performance of the demodulator. The effect of pulse carving is then shown to increase the penalty associated to PDf because of the optical filtering effect of the demodulator. Finally, a cost-effective calibration of the demodulator, reducing the impact of PDf by half, is proposed, and a new design approach further mitigating the PDf-induced penalty by 40 %.

Part 1 of the thesis will present the optical system testbed for ultra high speed long haul transmission, while Part 2 will present the analysis and reduction of PDf penalty in PSK demodulators. The organization of the thesis is as follows:

In section 1.1, the theoretical elements involved in the testbed design are reviewed. In section 1.2, the optical system components are described and selected; in section 1.3, the optical system design parameters are presented as well as design targets and optimization parameters driving to the final testbed implementation; in section 1.4, simulations are performed with DPSK, QPSK and DQPSK modulation formats to demonstrate the testbed functionality; and section 1.5 contains Part 1's conclusion.

In section 2.1, PDf is introduced; in section 2.2, the experimental setups and methodologies of the PDf penalty in a DPSK modulator are presented, in section 2.3, the experimental results are analyzed; and section 2.4 contains Part 2's conclusion.

References

- [1] G.P. Agrawal, "Lightwave Technology Telecommunication Systems", Wiley-Interscience, 2005
- [2] J.H. Franz, V.K. Jain, "Optical Communications: Components and Systems", Narosa Publishing House, 2000
- [3] S. V. Kartalopoulos, "DWDM, Networks, Devices and Technology", Wiley-Interscience, 2003
- [4] J. L. Miller, E. Friedman, "Optical communications rules of thumb", McGraw-Hill, 2003
- [5] K. Roberts, I. Roberts, "DSP: A Disruptive Technology for Optical Transceivers", IEEE European Conference on Optical Communication (ECOC), pp. 1-4, 2009
- [6] I. Aldridge, "High-Frequency Trading: A Practical Guide to Algorithmic Strategies and Trading System", Wiley & Sons, 2009
- [7] G. P. Agrawal, "Fiber-Optic Communication Systems", Wiley & Sons, 1997

1 Design of an optical system testbed for ultra high speed long haul transmission

1.1 Background Theoretical Review

Lightwave systems are the normal extension of microwave communication systems. The major difference between the two is the part of the frequency spectrum they operate. While microwave systems operate in the range of 1 GHz, lightwave systems operate at 100 THz. Because of this increase in the carrier wavelength, lightwave systems can achieve much higher capacities. In order to make the electrical to optical conversion, the optical carrier wave needs to be modulated. In recent years, there has been a lot of interest in finding the best modulation format for wavelength division multiplexing (WDM) long haul systems [1]. It was only natural to look at modulation formats that are successful in the microwave industry and try adapting them to the optical domain.

1.1.1 Modulation Formats

Before any modulation is applied, the carrier wave is in the form of a continuous wave and is described by the following equation

$$E(t) = \operatorname{Re}\left[\hat{e}A_{0}e^{i\phi_{0}}\exp(-i\omega_{0}t)\right] \tag{1}$$

where Re represents the real part, \hat{e} is a unit vector representing the state of polarization, A_0 is the amplitude, ω_0 is the carrier frequency and φ_0 the initial phase.

Similar to electrical communications, the data can be sent over the medium by modulating different parameters of the carrier wave. In the digital case, these modulation formats are classified in three major groups: amplitude shift keying (ASK) if the amplitude A_0 , is modulated, phase shift keying (PSK) if the phase ϕ_0 is modulated

and frequency shift keying (FSK) if the frequency ω_0 is modulated. Figure 1 shows an example of the modulated optical carrier for different modulation formats, ASK, PSK and FSK, when the data encoded is a clock signal.

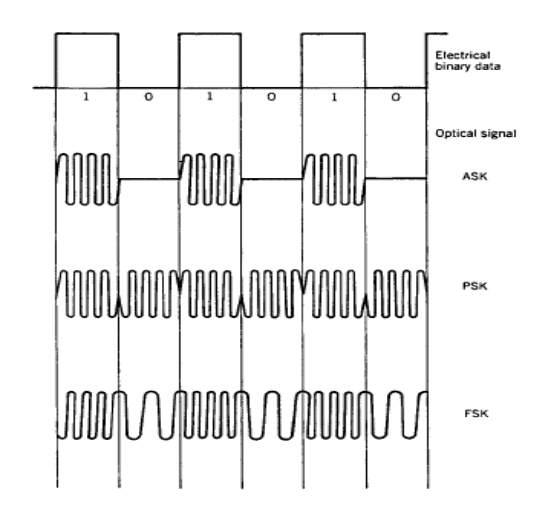


Figure 1 Modulated optical signal for ASK, PSK and FSK given a input electrical signal at the top [2]

1.1.1.1 ASK Modulation format

In the case of ASK modulation, the electrical field can be written as

$$E(t) = \text{Re}[A(t)e^{i\phi_0} \exp(-i\omega_0 t)]$$
 (2)

where the data is encoded directly in the amplitude A(t). In this context, A(t) is of the following form

$$A(t) = \sqrt{P_0} \sum_{n} b_n f_p (t - nT_b)$$
(3)

where P_0 is the peak power, $f_p(t)$ represents the optical pulse shape, T_b is the bit slot and b_n is the data and can take values of 1 and 0. Because the amplitude of the carrier wave is either high or low, the ASK modulation format is also called on-off keying (OOK).

The easiest way to generate an ASK optical signal, is to directly modulate the transmitting laser. By biasing the laser just below its threshold, the laser does not transmit any light. At each 1 bit, the laser goes over the threshold, emitting light for the duration of the bit. This method requires the laser to switch from on to off as fast as the bit rate. Although such lasers exist, this method is not viable at rates greater than 2.5 GHz [2]. The problem with direct modulation is that the laser chirps the sent signal. To make the laser switch from off to on state, population inversion is needed, accomplished by injecting more electron-holes pairs in the active region of the laser. This increase in carrier-charge density changes the refractive index of the active region, resulting in a time dependent change of the phase, which results in a frequency chirp. This chirp broadens the spectrum, which leads to temporal broadening.

A solution to the chirping problem is to use a Distributed Feedback (DFB) laser and externally modulating the continuous wavelength (CW) light. There are two external modulators used in lightwave systems. One modulator makes use of the electro-optic effect, by applying voltage on an appropriate material the refractive index can be changed, which changes the phase of the signal. The second modulator makes use of the electro-absorption mechanism. This type of modulator acts directly on the optical power of the signal in response to the applied voltage.

Since the data is coded in the signal's amplitude, ASK signals can be directly detected at the receiver by a square law device. A photo-detector transforms the intensity of the optical field to an electrical signal, thus recovering the data.

1.1.1.2 PSK Modulation format

In the case of PSK modulation, the electrical field can be written as

$$E(t) = \text{Re}[\hat{\mathbf{e}}A \exp(i\phi(t) - i\omega_0 t)] \tag{4}$$

where the data is encoded in $\phi(t)$. For binary PSK, BPSK, $\phi(t)$ takes two values, either 0 or π , and can be written as

$$\phi(t) = \sum_{n} b_n \pi f_p(t - nT_b) \tag{5}$$

where T_b is the bit period, f_p is the temporal profile of the optical signal and b_n represents the n^{th} bit. It is important to notice that for PSK modulated signals the optical power remains constant. Contrary to ASK, PSK modulation cannot be directly detected at the receiver since all phase information is lost using the direct detection technique. In this case, we need to use a coherent, either homodyne or heterodyne, decoding technique before the signal is detected, which converts phase information into amplitude information (see section 1.1.1.9 for discussion on coherent detection techniques).

A problem with BPSK modulation is that the phase needs to remain stable for the entire bit stream in order for the receiver to be able to recover the data. To address this problem, the differential PSK (DPSK) format was developed. In this case, the phase shift of the kth bit depends on the phase of the k-1 bit. DPSK format does not suffer of the phase-stability since the phase is differentially encoded between two neighboring bits; the phase only needs to remain unchanged for the two bit period.

Another flavor of the PSK format is the quadrature PSK (QPSK). In this modulation format is more spectrally efficient compared to BPSK. Two bits are encoded simultaneously to create one of the four carrier phase, 0, $\pi/2$, π and $3\pi/2$. QPSK uses half the bandwidth of BPSK because it reduces the bit rate by a factor of 2. As in the case of BPSK, this modulation format suffers from phase-stability problem. Here again, the phase can be encoded differentially between two neighboring bits obtaining the differential QPSK (DQPSK) format.

1.1.1.3 FSK Modulation format

In the case of FSK modulation, the electrical field can be written as

$$E(t) = \text{Re}[A \exp(i\phi_0 - i(\omega_0 \pm \Delta\omega)t)]$$
 (6)

where we either add or subtract $\Delta\omega$ if the data is 1 or 0, respectively. We can notice that by rewriting the argument of the exponential as $i\omega_0t+i(\varphi_0\pm\Delta\omega t)$, the FSK format becomes a special case of PSK, where the phase is increased or decreased linearly for all the duration of the bit period. An easy way of encoding the data as an FSK signal is to use direct modulation of the laser. As mentioned in section 1.1.1, there is a time-dependent phase shift with applied current. This frequency chirp can be encoded as a means of encoding the data. Although, the signal is easily encoded, the FSK format is rarely used in the industry because of the difficulties of extracting the data out of the frequency shifts.

1.1.1.4 Data formats

In optical digital communications, there are two types of data formats. They are differentiated by the length of the signal stays in a high state compared to the bit duration. The two formats are called Non-Return-to-Zero (NRZ) and Return-to-Zero (RZ).

1.1.1.5 Non-Return to Zero

In the case of NRZ, the pulse stays the same for the entire bit duration. In the case the data contains a train of 1, the modulated signal stays high for the entire period. In order to recover the data, a receiver needs to first extract a clock. This task can become

difficult if the data contains a long sequence of 1 or 0. An advantage of the NRZ format is that it requires half the bandwidth of RZ for the same bit rate. This can be explained by the fewer transitions in the case of NRZ format compared to RZ. As NRZ pulse occupies the entire bit period, it is more susceptible to inter-symbol crosstalk, thus can tolerate no pulse broadening. Also, as the average power is higher in NRZ, it is more subject to suffer from nonlinear effects. For these reasons, NRZ format is not used at data rates higher than 10 Gb/s [2].

1.1.1.6 Return to Zero

In the case of RZ, the pulse is high for anything less than the entire bit duration and returns to zero before the end of the bit period. As it can easily be seen, in the RZ format, all pulses are the same but the spacing between them depends on the bit pattern. An important quantity of the RZ format is the duty cycle and is defined as the ratio of pulse width to bit length, T_p/T_b . The most common duty cycle is 50% but for certain applications duty cycles of 66% or 33% are used. Compared to NRZ, RZ format suffers from less nonlinear effects and is more tolerant to pulse broadening.

1.1.1.7 Optical Signal

Most of the deployed 10 Gb/s lightwave systems are using the NRZ-OOK modulation format. As the data rates go beyond 10 Gb/s, the penalties from chromatic dispersion (CD), polarization mode dispersion (PMD) and nonlinear effects, become much greater than in traditional systems. There is a need to switch to new modulation formats that are more tolerant to such impairments. One modulation format is the RZ. As the pulse occupies a fraction of the bit period, it is more tolerant to pulse broadening. Also, for

the same average power, more signals with higher peak powers can be sent, thus improving OSNR. All these benefits come with a price in bandwidth; the RZ format uses twice as much bandwidth as NRZ. Further, to increase spectral efficiency, which is very low in current lightwave systems (0.2bit/s/Hz), we can use modulation formats as QPSK and DQPSK, which use two orthogonal carriers to effectively double the bandwidth. Furthermore, we can use two orthogonal polarizations to increase even more the spectral efficiency in modulation format as Polarization Multiplexed – QPSK (PM-QPSK) and Polarization Multiplexed – DQPSK (PM-DQPSK). An optical stream that uses PM-(D) QPSK as its modulation format with 50GHz channel spacing has a spectral efficiency of 1.6bit/s/Hs an increase of 8 times the current deployed systems. In the next two sections, the generation of the optical signal in different modulation formats and the recovery of the data at the receiver side are discussed.

1.1.1.8 Optical signal generation

In this section, the way that different modulation formats are achieved optically is investigated. A combination of Mach-Zehnder modulators is used to achieve this goal. Figure 2 shows a Mach-Zehnder modulator and its transfer function. Driving both arms of the modulator with data and data inverted make the modulator to operate in a push-pull configuration. Dual drive modulators have the driving voltage halved compared to the single drive modulators.

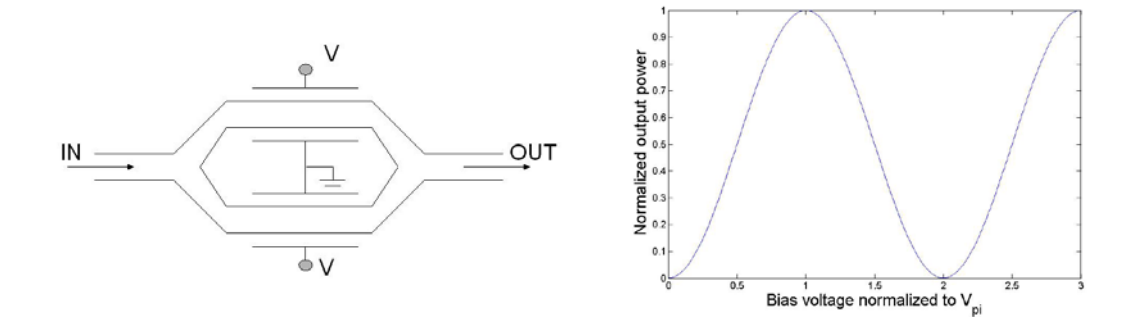


Figure 2 Mach-Zehnder Modulator and its transfer function [3]

The physical concept involves the creation of a phase difference between the two arms of the MZM by changing the index of refraction of each arm with the applied voltage. Mathematically, the equation describing the MZM is given in equation 7:

$$E_{out} = \frac{1}{2} \left(e^{-j\phi_1} - e^{-j\phi_2} \right) E_{in} \tag{7}$$

where, $\phi_1=(2\pi/\lambda)n_1L_1$ and $\phi_2=(2\pi/\lambda)n_2L_2$, where n and L are the refractive index and the length of each arm respectively.

The power transfer function shown in Figure 3 is obtained by squaring the electric field of (7) and interchangeably using the voltage controlling the index of refraction.

Generation of OOK is achieved by biasing the voltage in the middle of the linear regime and operating it over the linear regime of the MZM transfer function as shown in Figure 3.

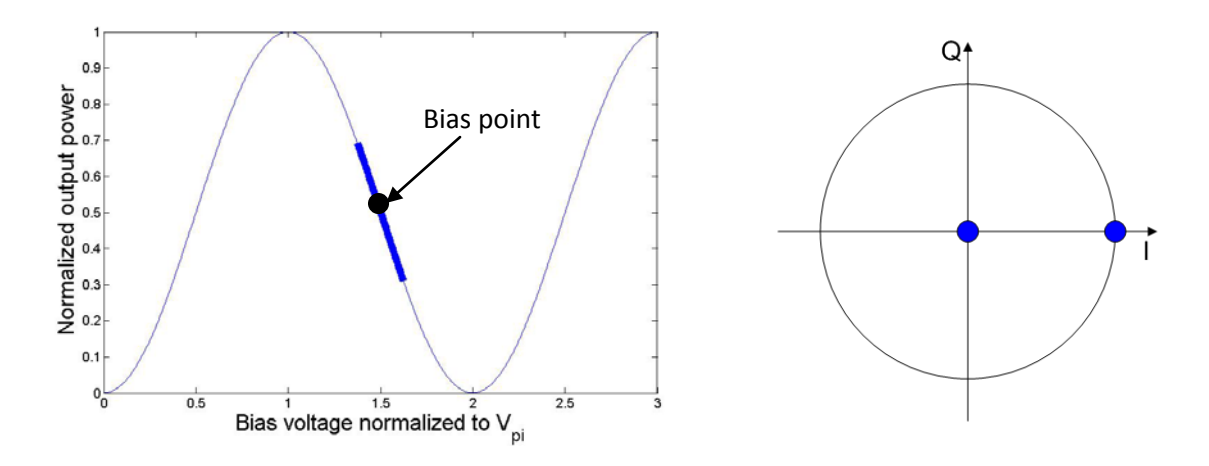


Figure 3 MZ transfer function showing the bias point and operation range of OOK (left), and the corresponding signal constellation (right)

To generate BPSK, the modulator is biased at its minimum and is driven by NRZ data with amplitude of $2V_{\pi}$ as shown in Figure 4.

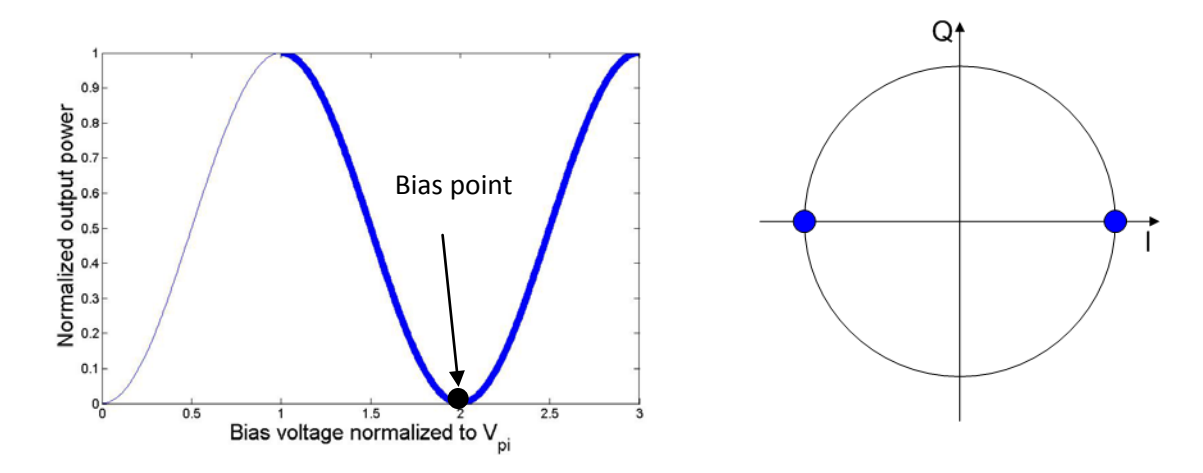


Figure 4 MZ transfer function showing the bias point and operation range of BPSK (left), and the corresponding signal constellation (right)

The NRZ data needs to be pre-coded first such that there is a 1 each time the data changes and a 0 if it remains unchanged. An interesting feature of the Mach-Zehnder modulator makes it very attractive for this application. Each time the modulator passes

through its minimum the output signal is shifted by exactly π . This can be understood from the angle of equation (7) and plotted in Figure 5.

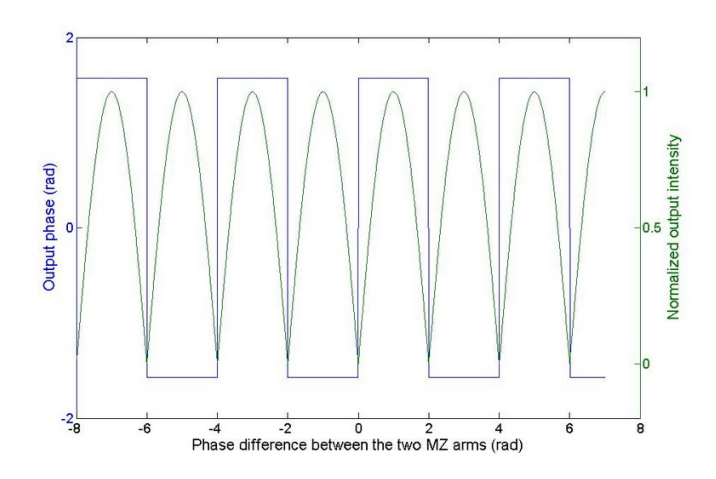


Figure 5 MZ output phase (rad) and normalized output intensity

To generate the optical stream in the QPSK format, two Mach-Zehnder Modulators are needed and a phase shifter. The two modulators are used to encode BPSK format. Using the phase shifter, one of the BPSK streams is shifted by $\pi/2$ to form the quadrature signal. The generation of the BPSK signal is very similar to the generation of the DPSK format described above, with the difference that the data is not pre-coded and the modulator is biased at $V_{\pi}/2$. The QPSK modulator is shown in Figure 6. The operation regime and bias points of each MZ are the same as those for BPSK (Figure 4).

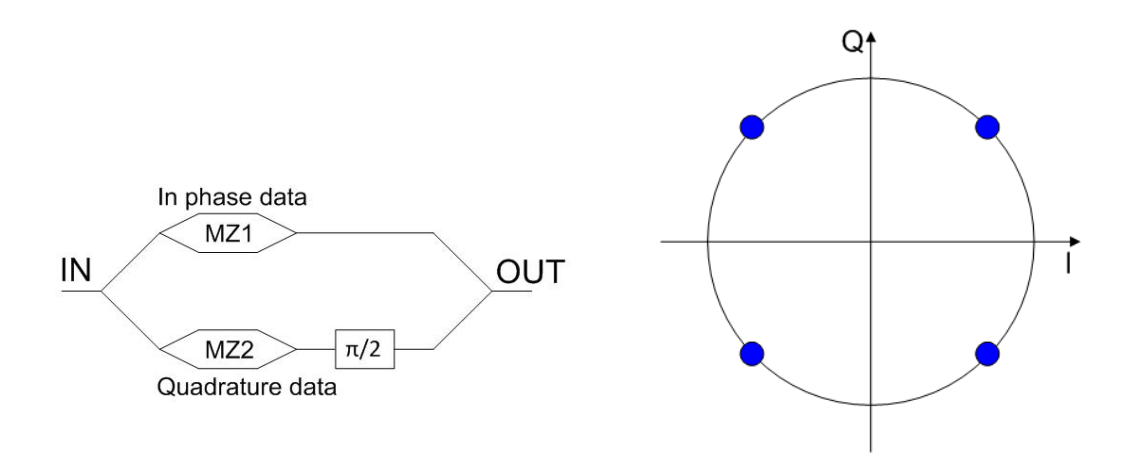


Figure 6 MZ transfer function showing the bias point and operation range of QPSK (left), and the corresponding signal constellation (right)

The RZ signal is obtained by an additional MZI called a carver (or a clock) and its purpose is to generate an optical pulse train at the desired bit rate. One possible operation range and the bias of the carver are shown in Figure 7. The carver is biased at its maximum and is driven by a sine wave with amplitude of $2V_{\pi}$ peak to peak and half the data frequency.

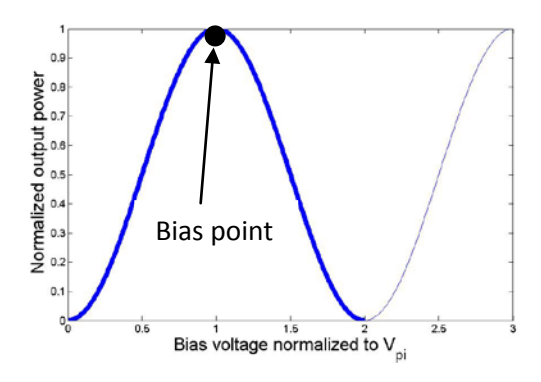


Figure 7 MZ transfer function showing the bias point when operating as a carver

The modulations used in the testbed were RZ-DPSK and RZ-DQPSK and their respective modulator setups are shown in Figure 8, where we can notice the additional MZ1 carver used for RZ modulation. Here again, the difference between the DQPSK format and the QPSK format is the pre-coding done on the data, while the hardware remains identical.

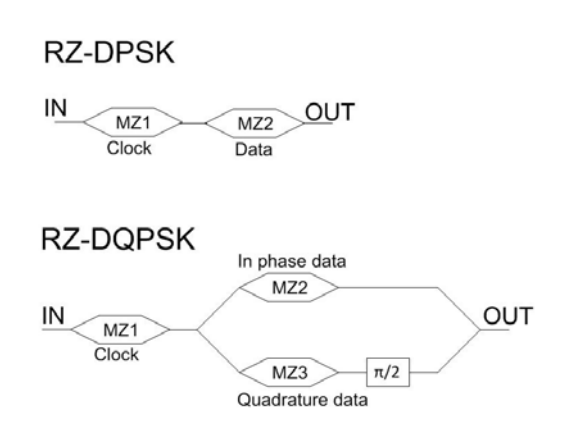


Figure 8 Modulator setups used for generating RZ-DPSK and RZ-DQPSK

1.1.1.9 Optical signal recovery

The optical frequency is too high to be able to convert and/or process the electric field electronically. The next best thing is to capture the photon's energy (square law detectors (SLD) generating electric current) but this technique only captures amplitude but not phase information. SLDs are sufficient for intensity modulated direct detection (IMDD) techniques since we are only interested in the amplitude of the signal. However, for phase modulation techniques, SLDs by themselves are insufficient since they are insensitive to phase.

For the special case of differential phase modulated signals, the data can be relatively easy recovered using delay interferometers (DIs). For example, in DPSK, a Mach Zhender

DI can be used, with one additional bit delay in one arm relative to the other arm, such that the phase in one time slot interferes with the differentially encoded successive time slot. As such, the data is converted from phase to amplitude modulation which can be converted to the electrical domain by the SLD. The recovery of the data out of the DQPSK signal is very similar to the procedure described above. The difference between the two is that in the case of DQPSK the signal has to be separated into its two orthogonal carriers. This can be achieved by adding a $\pm \pi/4$ phase shift in one of the branches of both Mach-Zehnder interferometers. Although the interferometer method used for differential formats is relatively easy to implement, only the phase encoded data is recovered, whereas all phase information related to the transmission in the optical fiber is lost in the process.

Whereas the interferometer method is only available for differentially encoded data, coherent methods are available for all phase encoded formats, differentially encoded formats included. Furthermore, the phase information related to the transmission in the optical fiber is recovered as well, allowing post processing mitigation of several optical fiber impairments, such as chromatic dispersion. In coherent heterodyne detection the conversion from phase to amplitude is accomplished by multiplying the optical signal of frequency f_c with a local oscillator (LO) laser of frequency f_{LO} . Both the signal and the LO hit the detector at the same time generating (among other DC or higher frequency filtered-out terms) a cross term at a frequency $f_c - f_{LO}$, from which both amplitude and phase information can be recovered. One challenge with coherent detection is manufacturing a LO whose linewidth is much smaller than $f_c - f_{LO}$ (which is in kHz or MHz scales). To overcome this difficulty, the same source is sometimes used to generate the signal and the LO, which is called homodyne detection.

1.2 Optical Link Components

The overall system can be seen in Figure 21. In this section, the different components are described and the type selection explained.

1.2.1 Transmitter

1.2.1.1 Laser

The system showed in Figure 21 uses 16 DFB lasers. A DFB laser diode is composed of an active region, also called gain medium, and a passive guiding layer where the index of refraction is varied to form a grating (Figure 9). The grating periodicity determines the emitted wavelength. The DFB lasers were chosen because they offer a very small linewidth and high enough power. The DFB lasers have a linewidth of 3MHz and could output up to 20mW of power. DFB lasers are usually used in both lab experiments and deployed commercially because of their low cost. For coherent detection techniques, the DFB lasers could be replaced by more costly external cavity lasers, which have much narrower linewidth, a crucial characteristic in coherent detection.

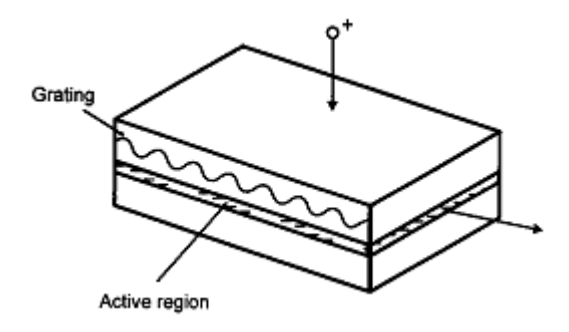


Figure 9 Distributed feedback, DFB, laser diode [28].

1.2.1.2 Modulator

Direct modulation is impractical for data rates above 10Gb/s for long-haul communication due to unintended phase changes in the carrier frequency as the current modulates the laser (chirp), and which generates pulse broadening as the signal propagates through the system. As such, an external Mach-Zehnder modulator was used to modulate the CW DFB laser. The Mach-Zehnder modulator is a structure containing a Mach-Zehnder interferometer and two phase modulators. The phase modulators are made of a material with strong electro-optic effect (LiNbO₃) which changes the phase of the optical field in response to the applied voltage. By combining two phase modulators in an interferometric structure, we can modulate the intensity of the optical stream. Figure 10 shows a Mach-Zehnder modulator. Driving both arms of the modulator with data and data inverted make the modulator to operate in a push-pull configuration. Dual drive modulators have the driving voltage halved compared to the single drive modulators.

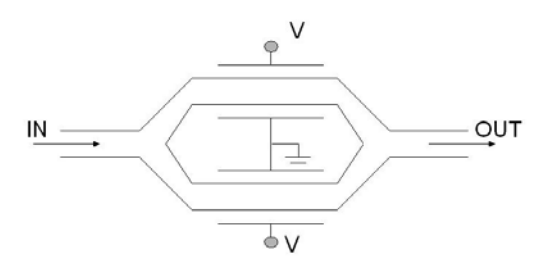


Figure 10 Mach-Zehnder Modulator

Some of the Mach-Zehnder modulators parameters are very important in the link design: extinction ratio, insertion loss and RF bandwidth.

1.2.1.3 Booster EDFA

The optical signal was amplified with a booster Erbium Doped Fiber Amplifier (EDFA). The main quality of a booster is to be able to amplify high power signals to send them down the transmission line. Its noise figure (NF) is not very important, since at this stage there is not much noise built in the signal. Another important parameter for all amplifiers is the gain flattness for different operating conditions. As such, all DWDM channels should be amplified by the same amount, and to accomplish that the gain ripple and gain tilt (the 2 parameters determining gain flattness) should be as small as possible in the optical power ranges used in the system. The optical power ranges should take into account that both single and multiple (maximum) channels experiments are intended in the future.

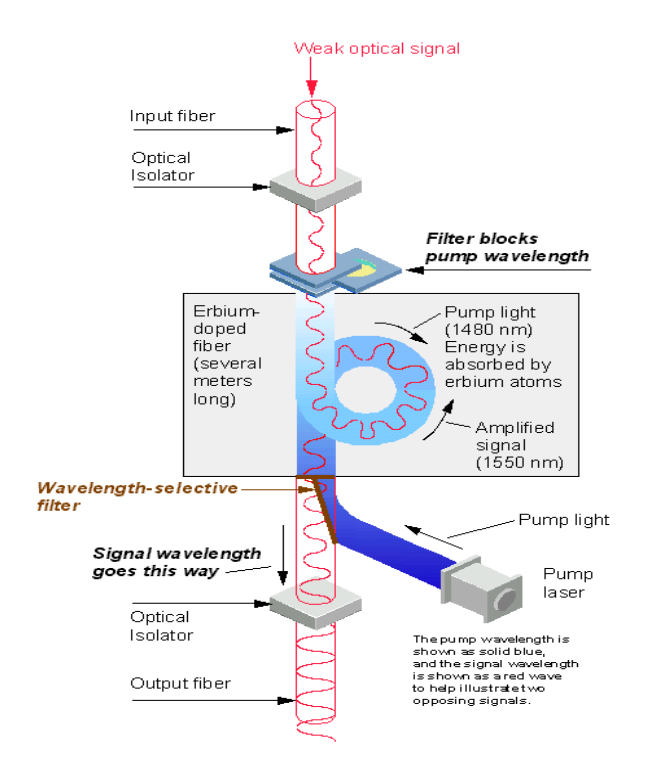


Figure 11 Erbium Doped Fiber Amplifier¹

¹ http://img.zdnet.com/techDirectory/_EDFA.GIF

There are 2 types of pumps used in EDFAs. The 980 nm band has a higher absorption cross-section and is generally used where low-noise performance is required. The absorption band is relatively narrow and so wavelength stabilized laser sources are typically needed. The 1480 nm band has a lower, but broader, absorption cross-section and is generally used for higher power amplifiers [29].

1.2.2 Transmission link

1.2.2.1 Optical Fiber: SMF vs. LEAF

The most deployed types of optical fiber in long haul systems are: Single Mode Fiber (SMF) and Large Effective Area Fiber (LEAF). LEAF fiber has lower dispersion and non-linearities. SMF was deployed traditionally but to reduce its dispersion (Figure 12) dispersion shifted fiber was deployed (DSF). Soon, research showed that a minimum amount of dispersion is needed to mitigate non linearities [2], giving rise to non-zero dispersion shifted fiber (NZ-DSF); the most popular NZ-DSF being LEAF. Both types were used in this thesis.

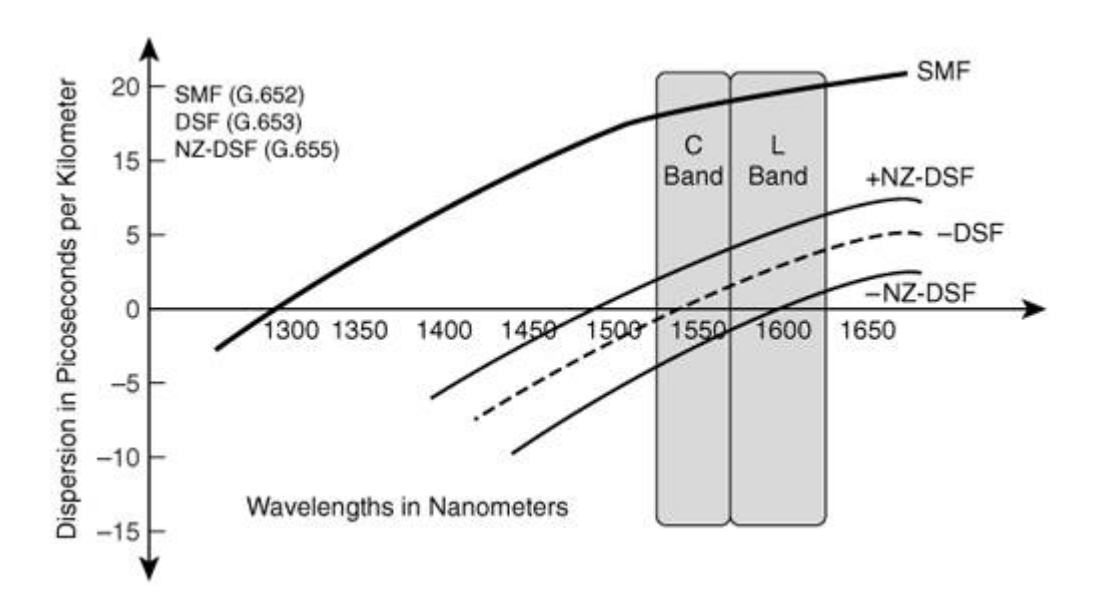


Figure 12 Different fiber types [30]

1.2.2.2 Inline EDFA

Inline EDFAs are used to compensate the loss incurred in the optical fiber. Each EDFA contributes to the noise accumulation in the link, but the impact is greater if the input noise in the amplifier is higher, a situation represented by the last amplifiers in the link. As such, the noise figure of the inline EDFAs needs to be fairly low. The same comments on gain flatness apply as in the case of the booster EDFA. Inline EDFAs come in two flavors: single stage EDFA and double stage EDFA with mid-stage access. The double stage EDFA design has a few advantages compared to the single stage design. The first stage is designed with a very low noise figure and is used to amplify the low input signals. It uses a 980nm pump as this pump offers a high absorption cross-section (see section 1.2.1.3). The second stage is designed for power amplification as the input signals to this stage have been already amplified. Two pumps are usually used: a 980nm forward propagating pump and a 1480nm backward propagating pump [2]. Because of the dual stage design, this type of EDFA offers a higher overall gain and lower noise figure compared to the single stage EDFA and is more suitable for long haul applications.

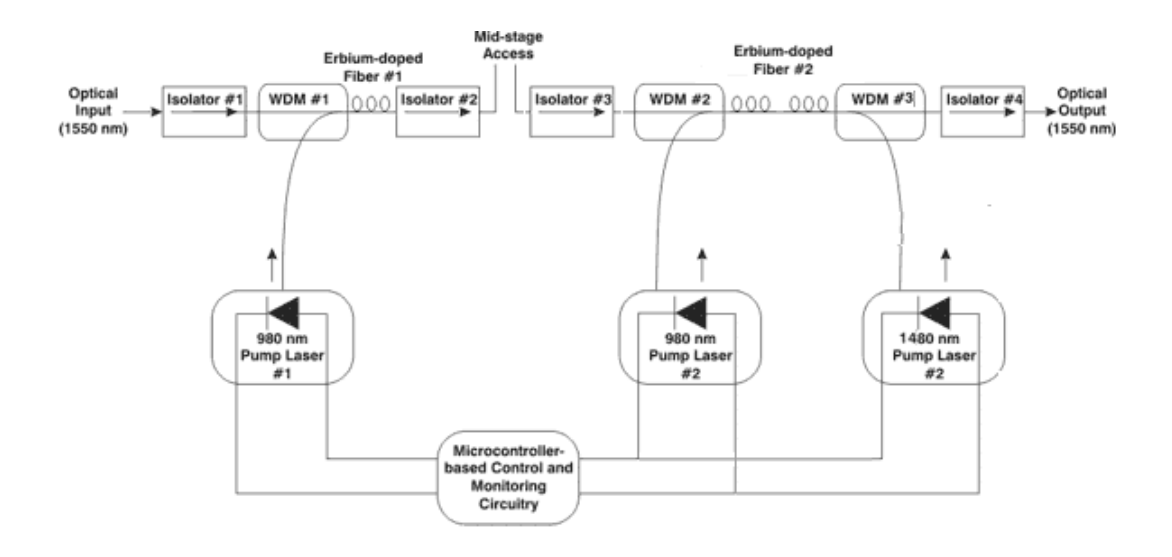


Figure 13 Dual stage Inline EDFA with mid-stage access [31]

1.2.2.3 Dispersion Compensation

In order to combat fiber dispersion, dispersion compensating modules (DCM) have been deployed. DCM types are matched to the type of fiber and the length of fiber used in the link. The main characteristic of DCM is to have the right amount of dispersion, but their Insertion Loss (IL) and Polarization Dependent Loss (PDL) should also be as low as possible. Even though electronic fiber dispersion techniques are starting to be used in the industry, the reality is that most existing systems employ optical DCM. Most common types of DCM are either dispersion compensation fiber (DFC) or fiber Bragg grating. DFC are optical fibers with negative dispersion coefficient. As a rule of thumb, the dispersion coefficient of DFC is negative and 10 times greater than the fiber it compensates [11]. Fiber Bragg gratings used as DCM have a chirped Bragg grating, such that lower wavelengths are reflected sooner by the Bragg grating and experience a shorter delay compared to the higher wavelengths. This effectively adds a negative dispersion to the system and compensates for the dispersion of the fiber.

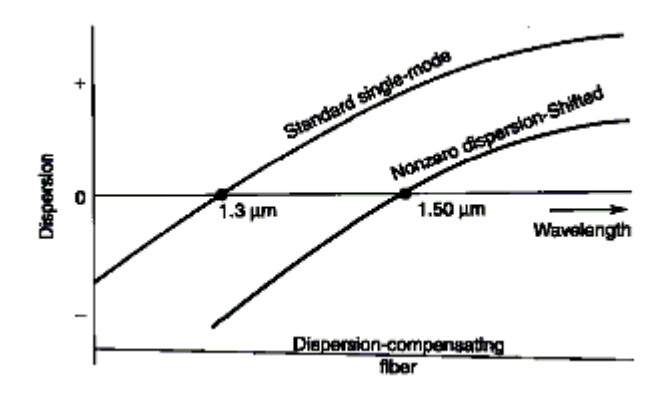


Figure 14 Dispersion compensation fiber characteristics²

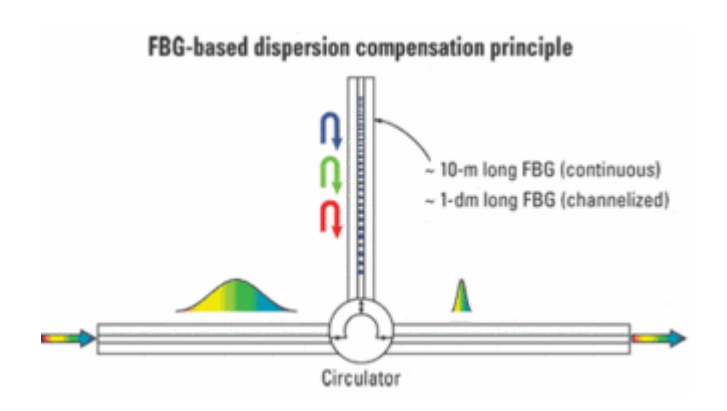


Figure 15 FBG dispersion compensation³

1.2.3 Receiver

1.2.3.1 Demodulator

The optical DPSK-modulated carrier was demodulated using a Mach-Zehnder delay interferometer (DI) with one additional bit delay in one arm relative to the other arm, such that the phase in one time slot interferes with the differentially encoded successive time slot.

² http://archive.electronicdesign.com/files/29/20891/fig2_web.jpg

³ http://zone.ni.com/cms/images/devzone/ph/6d573253317.gif

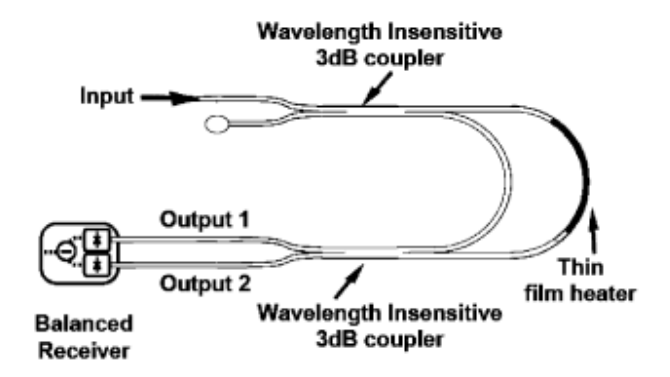


Figure 16: Schematic of the fiber-based DPSK demodulator by ITF Labs/Avensys.

1.3 Optical Testbed Design

1.3.1 Recirculating loops in literature

During the bibliographical research part of the thesis, the following testbed designs were found in the literature. The testbed in Figure 17 was used in the investigation of single channel 3R regeneration of a NRZ channel. It contains a transmitter receiver pair, 3 acousto-optic modulator (AOM) control switches, and a 100km loop containing EDFA every 50km spans, and a band pass filter (BPF). The experiment consisted of circulating a packet of light that filled the 100km loop and apply 3R regeneration after 100km, 500km and 1000km. In order to optimize of OSNR the power in the LEAF fiber and DCF fiber was set to moderately high, 5dBm and -3dBm, respectively. The authors used three optical switches, one to transmit the signal into the loop and the two others to switch between roundtrips with and without 3R regeneration. The authors found that optical 3R regeneration improved signal quality and extended the transmission length to more than 10000km. Although, regenerating the signal after every 100km is most beneficial, the authors demonstrated that even at distances of 500km the transmission length could reach 5000km.

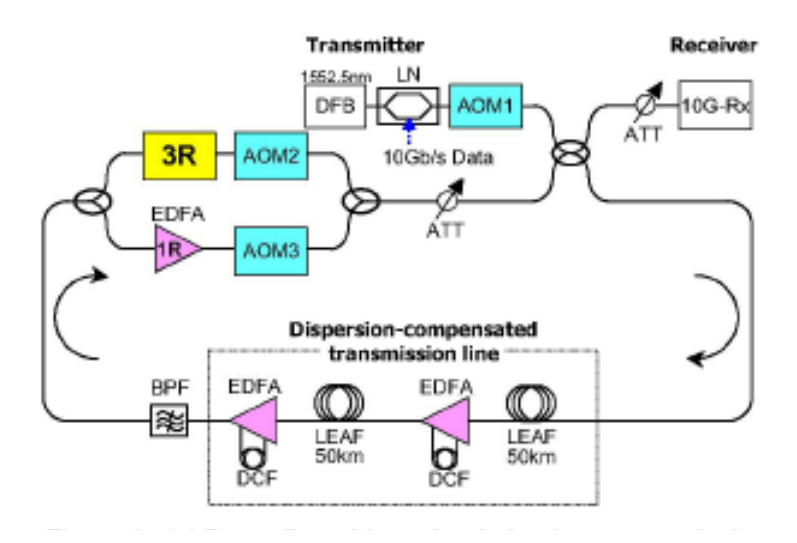


Figure 17 Reconfigurable recirculating loop transmission setup to enable cascaded 3R regeneration with a variable 3R regeneration spacing [32]

The testbed in Figure 18 was used in a multi channel experiment simulating 10Gb/s propagation. The authors use the optical recirculating testbed to investigate the influence on signal quality of cascaded optical nodes. The setup contains a transmitter receiver pair, a transmit switch and a loop switch, of variable length due to a variable optical attenuator, and variable EDFA spans. The two switches are operated by a pulse generator with two conjugate outputs. The length of the burst of the transmit switch is exactly equal to the time it takes the light to complete a full loop. This requirement is necessary to fill the loop with light and avoid EDFA transients (see 1.3.3.2). The authors used VPItransmissionMaker software for their numerical simulations. They proposed a simulation model that gave accurate results up to 250km.

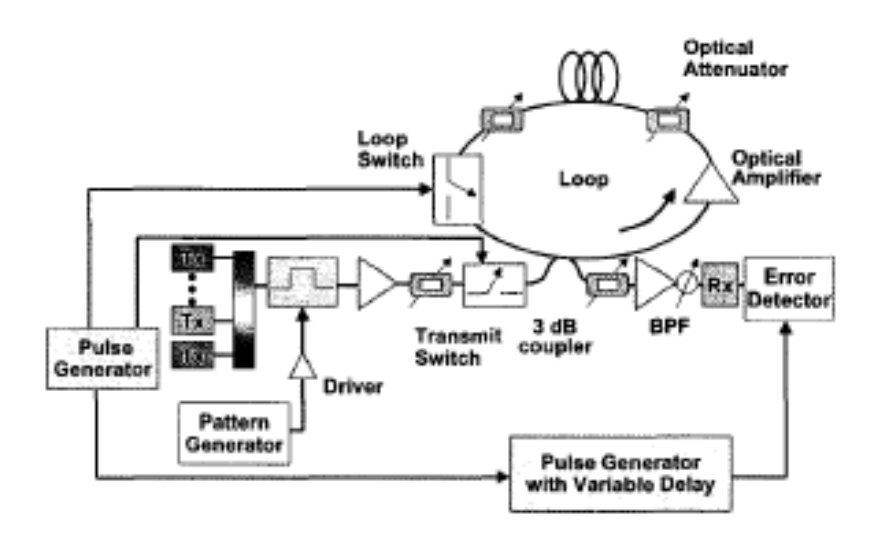


Figure 18 Experimental setup of the recirculating loop using two optical switches [33]

The loop in Figure 19 is used for single channel total stretched span of 4000km with Raman and EDFA amplifiers every 80km spans, and a loop length of 480km. It also contains a transmitter and receiver pair and 2 control switches. The scope of the experiment was to determine the maximal transmission length for a single channel at 170 Gb/s rate. Some key aspects of the testbed were the span loss of 19.3dB and span noise figure of 16.6dB. The authors used Raman amplifiers in the loop to minimize the span noise figure [34]. The optimum launch power was found to be between -1dBm and 0dBm depending on the transmission length. The OSNR after a full loop length (480km) was found to be 34.2dB.

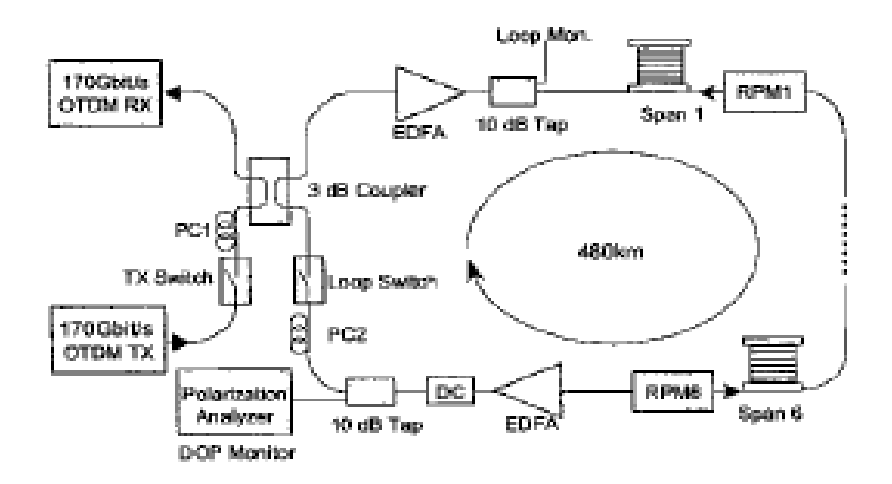


Figure 19 Recirculating loop setup for single channel 170 Gb/s transmission up to 4000km [34]

The loop in Figure 20 is used to investigate polarization effects in a dispersion managed system. It contains a single channel transmitter and receiver pair, a loop of 82 km, 2 control switches, polarization maintaining (PM) fiber and 2 polarization controllers (PC). One PC is to maintain the polarization in the receiver and a lithium niobate PC is used in the loop to simulate slow varying polarization effects in long haul optical fiber. The authors demonstrated that, by using a loop-synchronous polarization scrambling element, they could mitigate PMD effects for more that 650km of propagation.

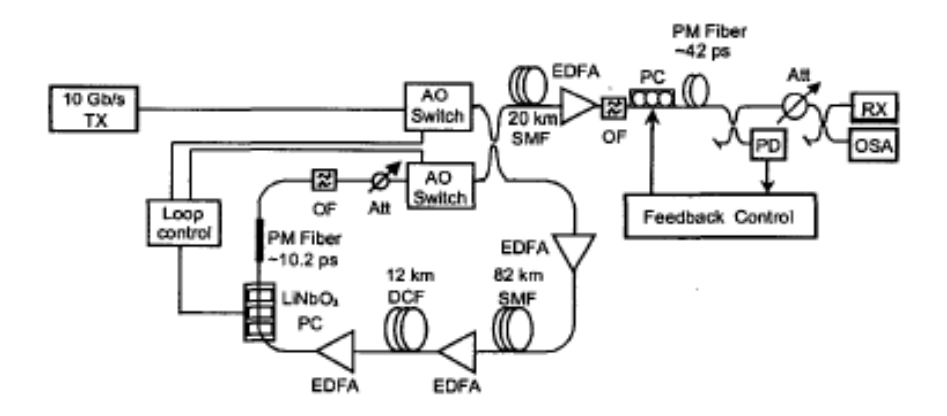


Figure 20 Setup of PMD compensation experiment using recirculating fiber loop with loop-synchronous polarization scrambling [35]

All these setups are very different and the differences are summarized in the following table.

Table 1 Comparison between 4 optical recirculating loop designs found in literature

Figure	Testbed purpose	Channels supported and optical filtering in the loop	Loop length (km)	Span size (km)	Number of control switches	Other elements
17	3R optical regeneration	1 channel and 1 BPF	100	50	2	3R regenerator
18	10G optical propagation simulation	Multiple channels and no filtering	Variable	Variable	2	Optical attenuator
19	170Gb/s 4000km long haul transmission	1 channel and no filtering	480	80	2	Raman amplifier
20	Polarization effects in recirculating loops	1 channel and 1 BPF	82	82	2	Polarization Controllers

It can be seen from Table 1 that the optical recirculating loops are very purpose specific. The 4 loops described have different lengths and use different purpose specific elements. However, there are some architectural traits that are common to all 4 examples. The first common element is the number and placement of control switches. In all 4 instances, the switches were placed right before the loop coupler, the transmit switch before the transmit side and the loop switch on the loop side. In most cases these switches are acousto-optic, since the switching speed is in the MHz range, and attenuation is in the 50dB range. This is opposed to MEMS switches which operate in the kHz range and have typical attenuation ranges of 20dB.

1.3.2 Optical recirculating loop proposed design

In this section, the proposed architecture for the optical recirculating loop is presented. The purpose of a testbed is to reproduce as close as possible the characteristics of a real system but with less equipment. The testbed is separated in three constituents: the signal generation, the loop and the receiver. There are 2 additional architectural elements which are included to control the passage of data between the 3 constituents mentioned above: a transmitter switch and a loop switch.

The system shown in Figure 21 constitutes the final solution of the recirculating loop testbed. In each of the following subsections, the choice and characteristics of each of the loop components is explained in the context of the design objectives.

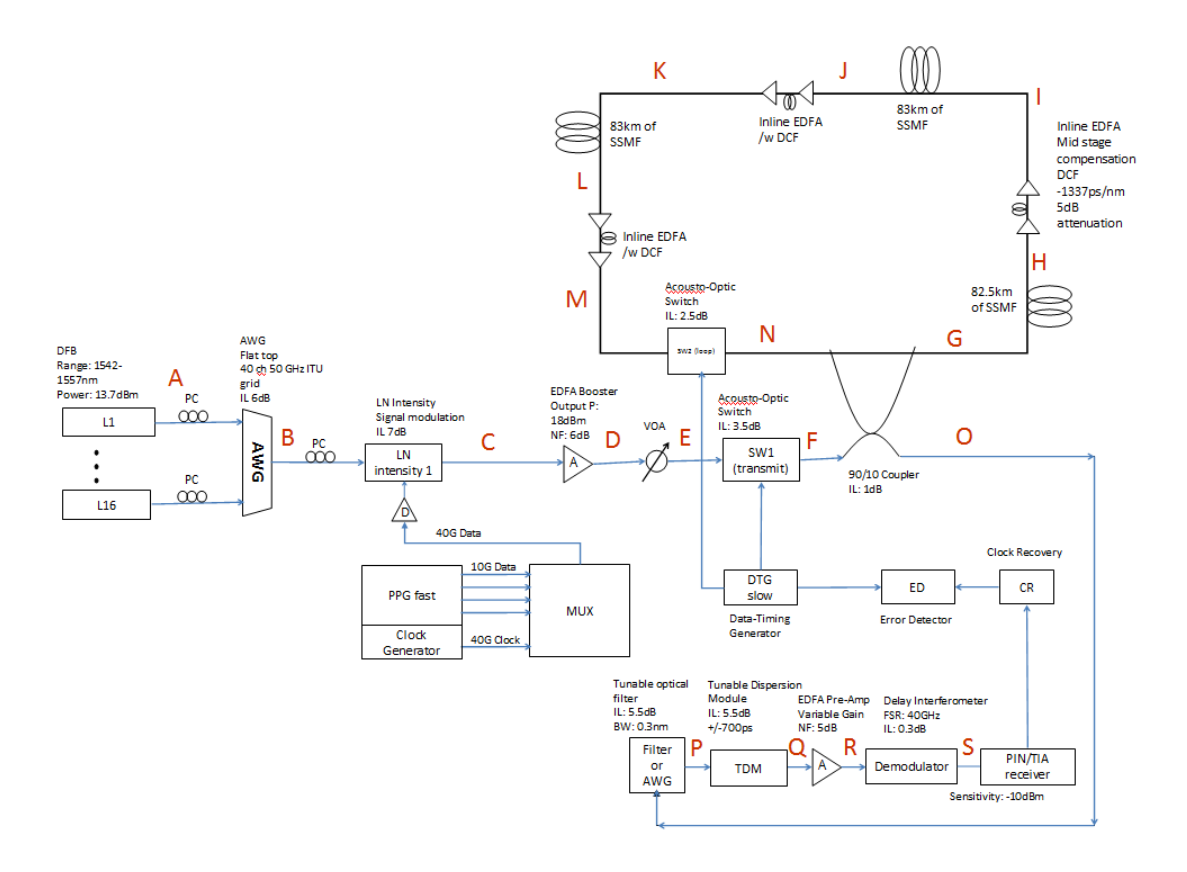


Figure 21 Optical Recirculating Loop using LEAF fiber with pre and post dispersion compensation

1.3.2.1 Transmitter

The final solution for the transmitter requires 16 channels, modulated at 40 Gb/s, on the 50GHz ITU grid. Also, the input of the loop the power should be -4dBm per channel (assuming worst case scenario), for a total power of 8dBm [39]. We have chosen -4dBm as our worst case scenario because it represents the signal input power of a NRZ modulated channel, the NRZ has the lowest tolerance to non-linearities amongst all the typical modulations analyzed in this thesis. As NRZ is the modulation format of 10 Gb/s systems, it constitutes a good starting point for the signal power level in the loop design. Given that the 90:10 loop coupler has an insertion loss of 10.5dB, the per channel power at the output of the booster should be 10dBm, and a total power of 22dBm for all the 16 channels. One criterion in the loop design was the maximization of the span length. As such, all extraneous losses were minimized; specifically the loop coupler was inserted with the 90 % arm in the loop, to reduce the loop loss due to the coupler to ~1dB. A 99:1 coupler was deemed unnecessary since the additional ~0.5dB reduction in loop loss was not warranted at the expense of an additional 10dB on the drop side.

The following lasers were already available in the lab:

192.45, 192.65, 192.75, 192.85, 192.9, 192.95, 193.2 THz.

In order to have a complete system of 16 channels on the 50GHz ITU grid the following lasers had to be bought:

192.5, 192.55, 192.6, 192.7, 192.8,193, 193.05, 193.1, 193.15 THz.

The above laser wavelengths were chosen to match the amplifier flattest gain spectrum in the C band.

The measured lasers output power varies between 12.5dBm and 13.7dBm.

These lasers are made by Nortel and they have a high output power. All the laser current drivers and TEC controllers were used to better match the optimal specs and tune the lasers on the ITU grid (See Appendix for laser specs). The DFB lasers were chosen because they offer a very small linewidth and high enough power. The DFB lasers had a linewidth of 3MHz and could output up to 20mW of power. For coherent modulation the lasers can be replaced with external cavity lasers (ECL), which have typical linewidths of 100 kHz.

The lasers were multiplexed with an arrayed waveguide grating (AWG) (See Appendix for AWG specs). The AWG was chosen over a regular DWDM multiplexer, because of its small insertion loss (IL).

The next component showed in Figure 21 is an optical modulator (See Appendix for modulator specs). Two Mach-Zehnder modulators were used to generate the different modulation formats.

Before the booster EDFA, there is around 13dB loss from the AWG and modulator (see Appendix for insertion loss (IL) of the AGW and modulator). The PDL of the modulator is used to make sure that the power per channel is equal in all channels, thus the power is equalized at the input of the recirculating loop, and thus, the total insertion loss of the modulator is not a fixed figure. As such, 16 polarization controllers are used, one for each laser. This technique is working for any type of lithium-niobate modulators. In [6], the authors use the same setup for two QPSK modulators generating 79 channels on the 50GHz spacing at 100 Gb/s.

A 40 Gb/s pulse power generator (PPG) and a SHF 40GHz radio frequency (RF) amplifier were used to drive the modulators (See Appendix for RF amplifier specs). As the V_{π} of the modulator is 5V and the output of the PPG is 1V the use of a RF amplifier to drive the MZM becomes mandatory.

The power per channel entering the booster EDFA is about -1dBm and for 16 channels, the total power is around 11dBm. The main quality of a booster is to be able to amplify high power signals to send them down the transmission line. Its noise figure (NF) is not very important, since at this stage there is not much noise built in the signal. In the lab we have a fixed output power booster from Optilab (See Appendix for booster EDFA specs). Optilab's booster EDFA is amplifying the 16 channels and the total output power is around 23dBm since this EDFA has a fixed output power. In order to get to the modeled 22dBm total power needed at the output of the booster, a VOA is used and it adjusts the power entering the transmission fiber.

The measured OSNR of the signal before entering the loop is 40dB. This value was measured for 1 channel. The typical value of the OSNR after the modulator is 50dB [37] and is directly linked to the RIN of the laser, which is the sole contributor to the signal noise at this stage. The only other contributors to noise are the optical amplifiers and they will add more noise as the signal propagates through the setup.

1.3.2.2 Transmission Line

For the transmission line models, three different types of fibers were used: older SMF, LEAF and new SMFe. The following parameters will change for each different type of fibre: the span loss, the nonlinear index and the PMD index. The PMD is a type of modal dispersion, where the two different polarizations of light travel at different speeds. It arises from imperfections and asymmetries of the optical fiber. At higher data rates, PMD limits the maximal transmission length. The ITU recommendations for 10-40Gbps long haul communications specify that the maximal PMD needs to be less than 0.2ps/sqrt(km) but common recommendations mention that at 40Gbps [36], the fiber needs to have a PMD index of less than 0.1ps/sqrt(km) [38]. As design parameters, we will only

consider the span loss, because it has a direct influence on the choice of inline EDFAs (See Appendix for SMF, LEAF and SMFe specs).

In the lab, the following fiber spools are available: 250km of old SMF and 300km of LEAF. Each of these spans has been used as the total loop length. Their span loss is between 24 and 25dB per 83km of old SMF and around 24dB per 100km of LEAF. The newer SMFe has a specified loss of 20dB (including connectors) per 100km of length. As a rule of thumb, the value of 24.5dB of loss per fiber span was used in the modeling of recirculating loop.

The modulation format directly influences the power entering the transmission line. The following four modulation formats were investigated: NRZ-OOK, NRZ-DPSK, RZ-DPSK and QPSK. NRZ-OOK was chosen as reference for the other modulation formats, since it represents the worst case scenario in terms of maximal power per channel (i.e. non-linear penalties). From the literature, it was determined that the maximal allowed power per channel for 40Gbps NRZ-OOK modulation is around -4dBm [39] in order to minimize the nonlinear effects in the fiber. The total power of 16 NRZ channels is 8dBm. Compared to NRZ-OOK, DPSK can accommodate an increase of 3dB in power per channel (due to the constant signal power level and the absence of steep bit transition slopes) [38, 41], DQPSK an increase of 1dB in power per channel (the two quadrature signals make DQPSK less robust to non-linear effects compared to DPSK) [38, 41] while RZ-DPSK can support an increase of up to 6dB in power per channel (as it benefits from the same effects as DPSK but also has a narrower pulse width, which makes this modulation more robust to non-linear effects) [40]. In this context, RZ-DPSK is considered as the other extreme of the system.

To calculate the maximal transmission length of an optical recirculating loop noise limited by EDFAs, we have used equation 8 as an approximation of the OSNR of the optical link [37]. To be accurate, the following assumptions must be true: all EDFAs have identical gains and noise figures, all span losses are identical, each EDFA compensates

for the loss of the previous span, the signal wavelengths is around 1550nm and we are using a laser with high OSNR (greater than 57dB).

$$OSNR_{dB} = 158.9 + P_{source,dBm} - \Gamma - NF - 10\log(B_r) - 10\log(N)$$
 (8)

where $OSNR_{dB}$ is the estimated OSNR in dB, the $P_{source, dBm}$ is the per channel input power in the loop in dBm, Γ is the span loss in dB, NF is the amplifier noise figure in dB, B_r is the optical measurement bandwidth in Hz and N is the number of amplifiers excluding the booster.

If the input power in the loop is -4dBm, with span losses of 25dB, a NF of 5.5dB and a bandwidth of measurement of 0.1nm, the signal can pass around 7 EDFAs so that the receiver OSNR to be greater than 15dB.

Three inline amplifiers were used at a distance of 80km of fiber span length, and allow going twice around the loop without regeneration. These amplifiers require a better NF than the booster, since this will limit the maximum transmission distance from noise build-up. The Optilab inline EDFA had a NF of 5.2dB (See Appendix for inline EDFA specs).

The system has to support a fully compensated transmission channel as well as a not compensated transmission channel (See Appendix for DCF specs). The loop design should permit a very flexible setup, allowing a great number of experiments in both compensated and uncompensated scenarios. For dispersion compensation, the two different dispersion maps which were used are showed in Figures 22, pre/post dispersion compensation, and 23, full inline dispersion compensation. These two dispersion compensation maps represent the two extremes of dispersion compensation networks architectures. The DCF requirement puts a requirement on the EDFAs to be a dual stage design and have a mid stage access. Thus, the addition of the inline compensation should not affect the performance of the loop. Additionally, the placement of the DCF needs to take into account the noise versus nonlinearities

tradeoff: if the DCF is placed at the end of the span, where power is low and nonlinear effects are minimal, the OSNR becomes much worse. As such, the best place to place the DCF is in the middle stage where the combined effect of nonlinearities and OSNR is optimal.

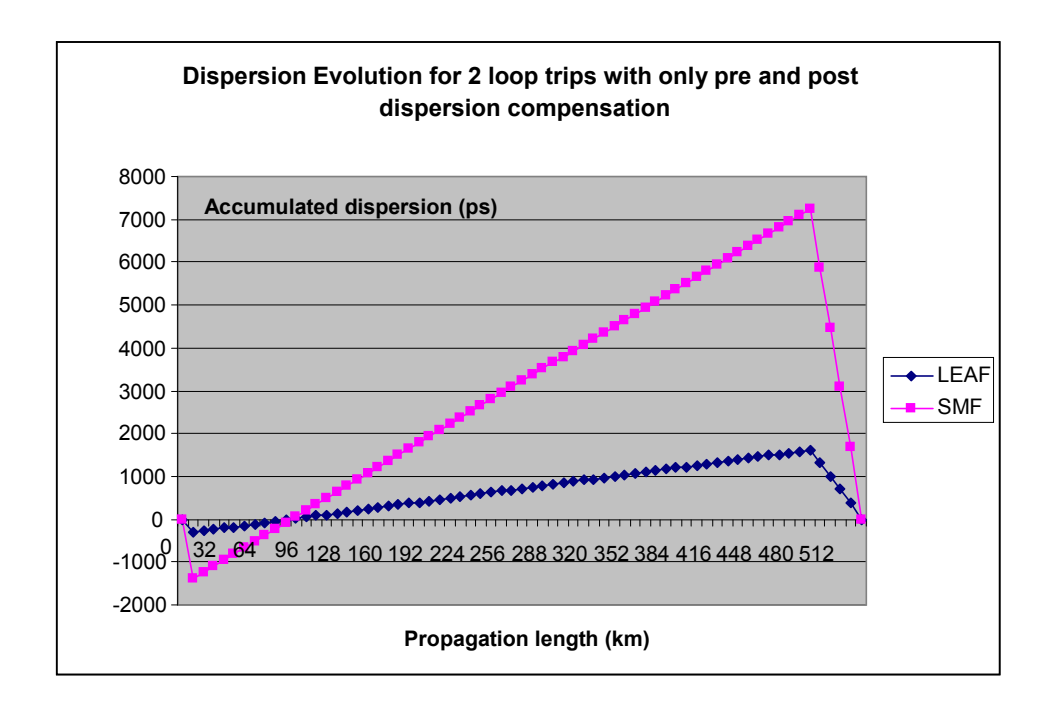


Figure 22 Simulation of the dispersion Evolution for two loop trips using only pre and post dispersion compensation for two different fiber types, LEAF and SMF

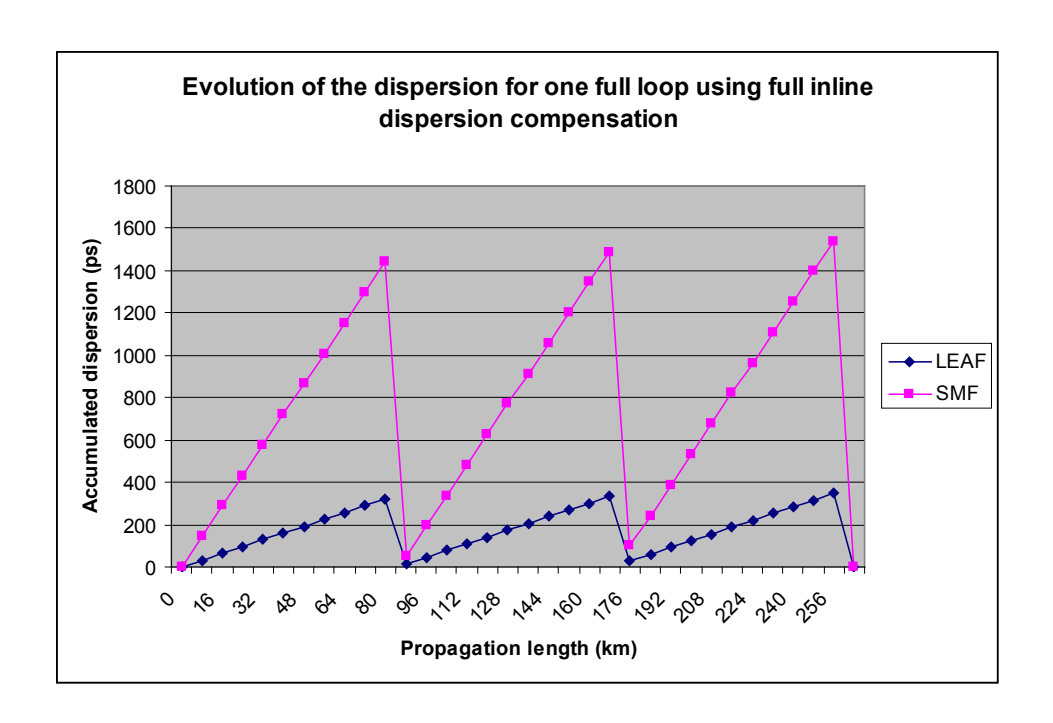


Figure 23 Simulation of the dispersion evolution for one full loop using full inline dispersion compensation for two types of fibers, LEAF and SMF

Given the above mentioned requirements, there are two extreme cases in terms of input power levels in the EDFAs: NRZ-OOK with old SMF and RZ-DPSK with new SMFe.

Below, case 1 represents the lowest power per channel that would enter the EDFA given the modulation with the lowest power requirements and the highest fiber type loss. Case 2 represents the highest power per channel that would enter the EDFA given the modulation with the highest power requirements and the lowest fiber type loss. These 2 extremes cases define the input power ranges of the inline EDFA which should experience a flat gain profile.

Case 1: NRZ with old SMF

At the input of the fiber span, the optical power per channel is at -4dBm. After 83km of old SMF the power per channel is minimal at -29dBm for a total power of -17dBm. The first two EDFAs need to provide 25dB of gain in order to fully compensate the loss of the

fiber. The last EDFA needs to provide 28dB of gain in order to compensate for the span loss plus the insertion loss of the switch and coupler. The maximal total output power that an EDFA has to provide is 11dBm.

Case 2: RZ-DPSK with new SMFe

At the input of the fiber span, the optical power per channel is at 2dBm. After 100km of SMFe the power per channel is minimal at -18dBm for a total power of -6dBm. The first two EDFAs need to provide 20dB of gain and the last EDFA 23dB of gain. The maximal total output power that an EDFA has to provide is 17dBm.

The two above mentioned extreme cases put certain system requirements on the inline EDFAs. The EDFAs needs to allow input powers of -29dBm and provide a minimal gain of 28dB, such that the output is still flat and the noise figure within acceptable limits (6dB). Also, the maximal output power has to be greater than 17dBm.

1.3.2.3 Receiver

A matched AWG on the 50GHz ITU grid was used to select the different channels under observation. The filtering was done before the amplification, to clean the signal of unwanted noise. A tunable dispersion module was used to compensate for the residual dispersion in the signal. This module can compensate from -700 to 700ps. Only one wavelength at a time was compensated, thus optimal compensation is achieved, i.e. the dispersion compensation required to maximize BER.

The pre-amplification used a pre-amp EDFA (See Appendix for preamp specs), which has a very low noise figure and can amplify very low signals. The pre-amp EDFA has a NF of 4.3 dB. To convert the optical signal to an electrical signal, PIN photodetectors were used (See Appendix for photo-detector specs). The important figures of a PIN

photodetector are its responsivity, defined as the output current per received power (A/W), and its sensitivity, the minimum amount of received signal power to guaratee a certain BER performance. The photodetector had a responsitivity of 0.35V/W and a sensitivity of -9dBm for a BER of 1E-10.

The receiver was using a 40Gb/s error detector, which was used to measure the BER.

1.3.2.4 Control switches and loop synchronization

The first control element is the transmit switch which is placed right before the loop coupler on the transmitter side of the coupler (See switch 1 in Figure 21). It controls the packet length sent into the loop to prevent successive packets interference in either the loop or the receiver. The packet length is defined as the time it takes light to travel once around the loop. Data cannot be sent continuously in the loop for a longer time than the packet length since it would interfere with the beginning bits of the stream. The transmit switch basically stops future packets from entering the loop until the current packet exits the loop and has been completely detected. Were this not the case, mixing of data in the loop or at the receiver occurs. The second control element is the loop switch, which is also placed right before the loop coupler, but on the loop side (See switch 2 in Figure 21). The purpose of this switch is to control the total propagation length of the each packet of light, by basically controlling the number of turns around the loop. In order for the loop to work, both switches and the error detector in the receiver need to be synchronized by the same clock. A timing data generator with multiple synchronized channels was used to generate the control signals of the switches and the error detector (Figure 21, DTG component).

1.3.2.5 Power Evolution

The following table summarizes the calculated power evolution in the system using the components readily available in the lab as reference.

Table 2 Signal power evolution recirculating twice around the loop

Tx						
Stage	Component	Gain/ Loss (dB)	Total Power (dBm)	Channel Power (dBm)	OSNR (1 st pass/ 2 nd pass)	Notes
A	DFB Lasers	NA	24	12		We are using 16 DFB lasers each outputting 12dBm
В	AWG	-6	18	6		40 channels 50GHz ITU Grid
С	LN Modulator	-7	11	-1		Intensity LN modulator
D	EDFA Booster	11	22	10	40	Fixed output power at 18dB has a boosted mode at 23dB
Е	VOA	var.	var.	var.		
F	AO Switch	-3.5	NA	NA		
G	90/10 Coupler	-10.5	8	-4		Loss measured between the transmitter branch of the coupler and the branch entering the loop.
Line						
G	Input to the loop	NA	8	-4		Depending on modulation desired input power from -4 to 0 dBm
Н	SMF span1	-25	-17	-29		Worst case scenario using old SMF
I	Inline EDFA	25	8	-4	23.4/17.4	With mid- stage access for DCF compensation (0 to 7.5dB loss)
J	SMF span2	-24.7	-16.7	-28.7		Worst case scenario using old SMF

К	Inline EDFA	24.7	8	-4	20.4/16.4	With mid- stage access for DCF compensation (0 to 7.5dB loss)
L	SMF span3	24	-16	-28		Worst case scenario using SMF
M	Inline EDFA	28	12	0	18.7/15.6	With mid- stage access for DCF compensation (0 to 7.5dB loss)
N	AO Switch	2.5	9.5	-2.5		,
G	Input to the loop	NA	8	-4		Gain of the loop is 0
0	90/10 Coupler	11	-3	-15		Output at 10% power port
Rx						
0	Input to the receiver	NA	-3	-15		From loop
Р	Tunable optical filter	5.5	-20.5	-20.5		BW 0.3nm, tunable over the C band (same power loss for AWG)
Q	Tunable dispersion module	5.5	-26	-26		-700 to 700ps compensation
R	EDFA Preamplifier	26.3	0.3	0.3	15	NF: 5dB. (See Appendix)
S	Delay Interferometer	-0.3	0	0		Output going to balanced detector

1.3.3 Experimental Methodologies

In this section, several experimental methodologies pertaining to the recirculating loop design are explained. These methods were perfected during the experimental implementation of the loop and the description below constitutes a procedural guide.

1.3.3.1 Recirculating loop power re-calibration

One important method used during the recirculating loop setup was the adjustement of the power levels entering and exiting the EDFAs. These EDFAs did not have a constant gain feature to ensure that the gain around the loop is constant independent of input power conditions and equal to OdB. If the gain is not OdB, each trip aound the loop would either amplify or attenuate the signal, reducing the usability of the setup for longer transmission distances. In order to achieve optimal BER, the VOAs need to be adjusted in order to keep the power entering the loop and the effective amplifier gain optimal. For each modulation format investigated, the optimal powers, hence the optimal VOA settings are modulation format specific. One inherent loop characteristic is ring feedback. As such, changing one power level affects both the power levels in subsequent stages as well as the self power for the next trip around the loop. To circumvent this issue, the power recalibration is performed with the loop control switch set to open. This effectively removes the ring feedback generated power instability, such that the VOA is adjusted to the desired stable point in one iteration.

1.3.3.2 Synchronization of control switches and error detector

The most important timing characteristic of the recirculating loop is the optimal packet length; defined as the packet length that fills the loop (i.e. the first bit in the packet exits the loop at the same time that the last bit enters the loop). If the packet length is longer than the optimal packet length, interference arises, while shorter packet lengths signify high power variations in the system between sequential packets. For example, in a 300km recirculating loop, the optimal packet length is in the ms (i.e. 10^{-3}) timescales. It will be shown below that the optimal packet length in our loop was found to be 1.4ms. A packet of 2ms would interfere with itself after passing through the loop, whereas a packet of 1 second would generate a continuous toggling between 1ms of light and 0.4ms of dark in the loop. This is unacceptable since the power in the loop needs to be kept constant in order to reduce EDFA transients, which would otherwise artificially impact the measurements.

The optimal packet length is the reference for all the controlling data timing signals. There are 5 timing signals controlling the proper functionality of the setup: the transmit switch signal, the loop switch signal, the error detector integration time signal, the

pattern repetition signal, and the data timing generator (DTG) clock. Figure 24 shows an example of the timing diagram for a 2 trips around the loop. The transmit switch signal, the loop switch signal, and the pattern repetition rate are multiples of the optimal packet length. The transmit switch signal is the time to generate the optical packet length. The loops switch signal is the number of times the signal must travel around the loop multiplied by the optimal packet length. The pattern repetition rate is the transmit switch time plus the loop switch time. The error detector integration time needs to be less than the optimal packet length minus the rise time and the fall time of the acousto-optic modulators (AOM).

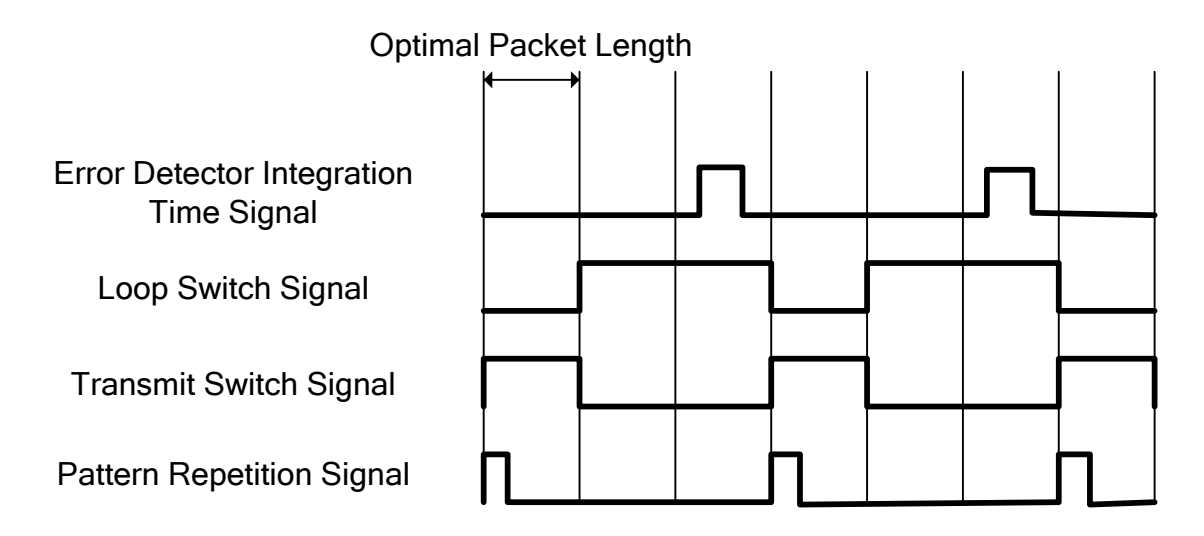


Figure 24 Data timing diagram showing the logical signals controlling the recirculating loop

1.3.3.3 Measuring eye diagrams with a recirculating loop

In order to obtain an eye diagram or the pattern shape with an oscilloscope, there is one requirement: the number of clock cycles generating the optical packet length (defined in section 1.3.3.2), in the data timing generator, needs to be a multiple of the PRBS length generated in the PPG. For our specific loop, the system is synchronized with the master

clock generator running at 40 GHz. This clock is then distributed to the PPG. Using the master clock, the PPG generates the DTG clock, which in turn is used to generate all the controlling data timing signals. The formula to calculate the optimal packet length is:

$$OptimalPacketLength(DTG_ClockCycles) = floor \left(\frac{LoopLength(s)}{DTG_Period(s) * PRBS_Length(bits)} \right) \tag{9}$$

For example, a 2^7 PRBS data stream generated by the PPG, and for a loop length of 1.4ms, and for a DTG clock of 10MHz, would require a optimal packet length of 13952 DTG clock cycles instead of 14000 DTG clock cycles, which is the full loop length. The 13952 DTG clock cycles amount to 1.3952ms, i.e. a difference of 5ns with the full loop length. The 5ns is much smaller than the EDFA transients timescales of ms, thus has no impact.

Once this condition is met, both the eye diagram and bit pattern visualization are possible.

1.4 Simulation Results

In this section, we perform a sensitivity analysis of the recirculating loop setup's BER on several parameters, such as input power in the spans, noise and non-linearities. For the sensitivity analysis absolute results are un-important; as such, the results below are discribed in a best case scenario, where the sensitivity of the BER on the various parameters is analysed.

In this section, we will present the result of the simulation done with the Optiwave sofware. The simulated testbed is exactly the one described in section 1.3.3. We have modeled two different modulation formats, DPSK and QPSK. Also, we have simulated the two dispersion maps described in section 1.3.3. The purpose of the simulations was to show that the proposed design would work with the established parameters, that is, a system that would support 16-32 channels at 40 Gb/s operating with error free (BER <

1E-9) or FEC error free (BER < 1E-3). The simulations did not try to minimize the BER of each dispersion map with modulation pair, and was not meant to be a comparison between the different setups.

In Figure 25, we see the eye diagrams of the received signal after transmission of 16 channels at 40 Gb/s through 600km (i.e., 2 loop lengths) of fiber for a NRZ-DPSK modulated signal. The optical channels were in the C band with 50GHz channel spacing.

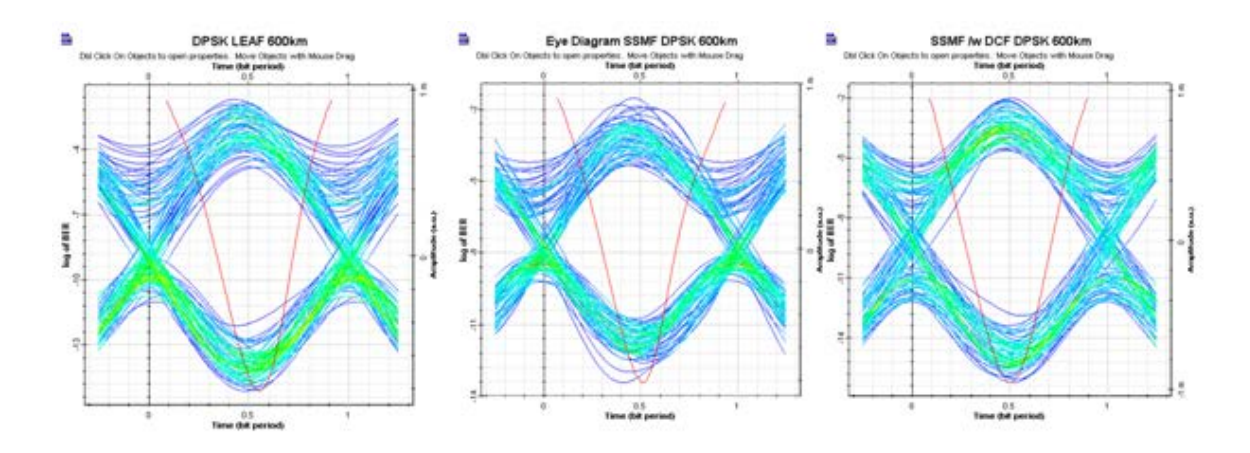


Figure 25 Optiwave simulation results. Eye diagram of 16 co-propagating channels at 40Gb/s after 600km transmission, 50GHz channel spacing, DPSK - LEAF fiber (left), SSMF (center), SSMF /w inline DCF (right)

The minimum BER for the three dispersion maps is 1.4E-15 in the case of LEAF fiber, 4E-14 in the case of SSMF and 1.12E-16 in the case of SSMF with inline DCF. The per channel powers used in the simulations were 0dBm for all three cases: LEAF, SSMF and SSMF with inline DCF. These BER numbers are very low compared to experimental values. The optical simulation program is calculating these BER from the estimated Q-factor of the eye diagram. We can see that for error free signals, the simulation program is not generating very accurate results.

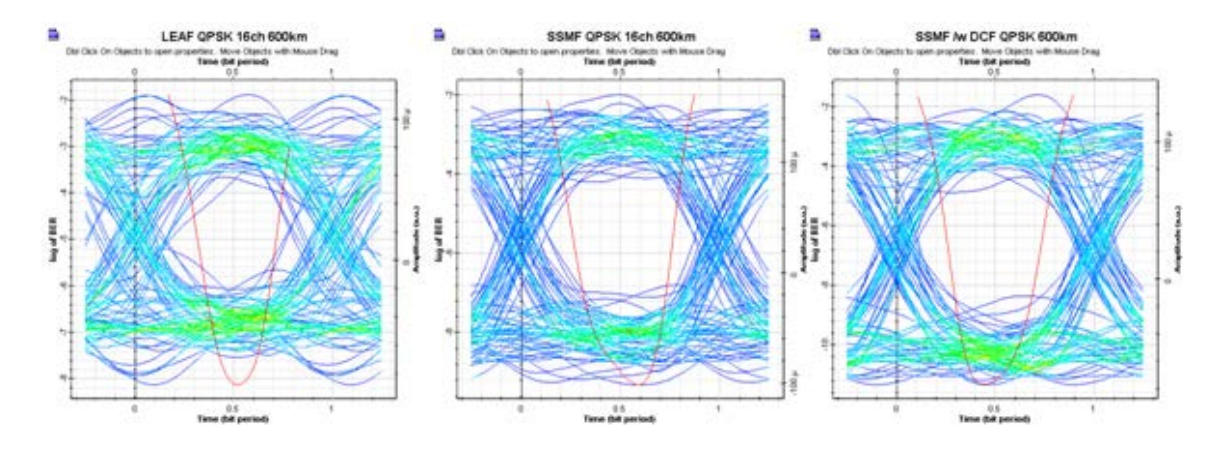


Figure 26 Optiwave simulation results. Eye diagram of one of the 16 co-propagating channels at 40Gb/s after 600km transmission, 50GHz channel spacing, QPSK - LEAF fiber (left), SSMF (center), SSMF /w inline DCF (right)

In Figure 26, we see the eye diagrams of the received signal after transmission of 16 channels at 40 Gb/s through 600km of fiber for a QPSK modulated signal. The optical channels were in the C band with 50GHz channel spacing. The per channel powers used in the simulations were -2.5dBm for all three cases: LEAF, SSMF and SSMF with inline DCF. For the QPSK modulation format, the BER for the three setups was 6.72E-9, 6.3E-10 and 5.74E-12 for LEAF, SSMF and SSMF with inline DCF, respectively.

Analyzing these results, we see that SMF is better suited for long haul transmission systems when compared to LEAF. As SMF has more dispersion compared to LEAF, it is more robust against non-linear effects. If we also compare the different dispersion maps, inline compensation vs. only pre/post compensation, inline compensation is better suited for our setup. As the DCF has a small effective area [11], it suffers more from non-linear effects compared to regular fiber. As we are using one EDFA to compensate for the majority of DCF power losses in the pre/post compensation scheme, the input power in the DCF is higher compared to the inline compensation scheme, where the DCF is inserted in the mid-stage of each EDFA. As such, pre/post compensation suffers more from non-linear effects, as seen by the higher BER compared to inline compensation.

In Figure 27, we can see the eye diagrams of the received signal after transmission of 16 channels at 40 Gb/s through 1800km of fiber for a 50% RZ-DPSK modulated signal. We chose the RZ-DPSK as modulation format, as it has a good balance between robustness to impairments and total cost of solution implementation. The optical channels were in the C band with 100GHz channel spacing. As the bandwidth of a 40 Gb/s 50% RZ-DPSK is 80GHz, we could not fit them in a 50GHz window. In this case, the minimal BER achieved was 1.58E-6 for LEAF, 2.5E-7 for SSMF and 4.2E-10 for SSMF with inline DCF. We can notice that our setup using SSMF with inline DCF achieved error free operation even after 1800km. The per channel powers used in the simulations were -3dBm for all three cases: LEAF, SSMF and SSMF with inline DCF.

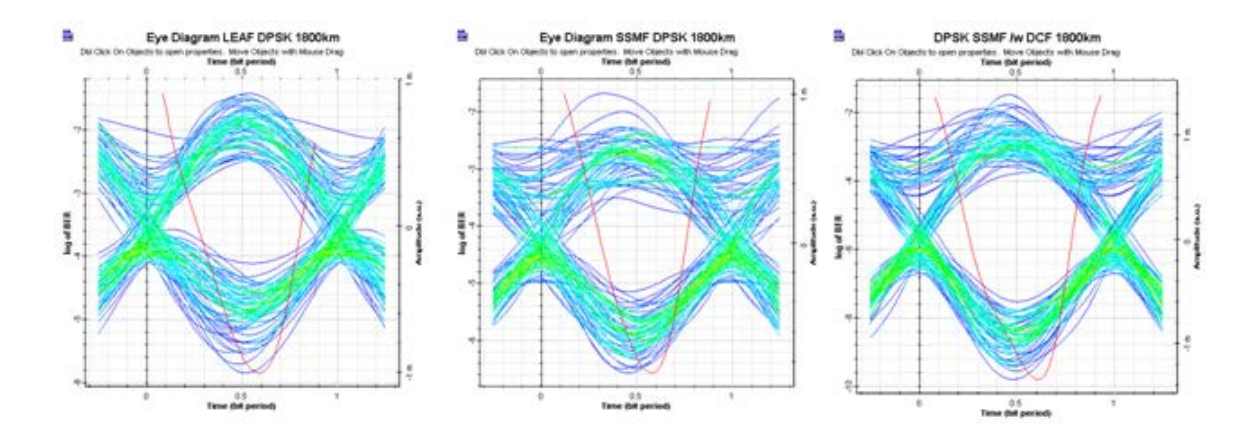


Figure 27 Optiwave simulation results. Eye diagram of 16 co-propagating channels at 40Gb/s after 1800km transmission, 100GHz channel spacing, DPSK - LEAF fiber (left), SSMF (center), SSMF /w inline DCF (right)

1.5 Experimental results and setup improvement considerations

The optical recirculating loop shown in Figure 21 was put together with the available parts. The experimental setup consisted of 1 channel at 10Gb/s with a wavelength of 1550nm, using OOK and DPSK modulation and in line dispersion compensation. Our setup used an old SMF which had an O.3dB/km measured loss, including connectors.

The loop consisted of three span lengths of approximately equal length of 83km. We have used acousto-optic modulators (see Appendix for specs) as loop switches and five Optilab EDFAs (1 booster, 1 pre-amplifier and 3 inline).

The first experiment consisted of measuring the best BER at the receiver after 1 loop length, a straight line experiment of 250km. After optimizing the power of the signal entering each span, by adjusting the gain of each amplifier with mechanical optical attenuators, the best BER for OOK was 6.53E-04 for an input power of -3.5dBm and for DPSK 7.31E-6 for an input power of -2dBm. After investigation, we have found the sources of our poor BER results: 1) the input power to the inline EDFAs was too low (i.e. -27dBm/channel) and 2) the amplifiers were generating a lot of ASE (even though they were spec'ed – see Appendix – to support these power levels with low noise). After the addition of 7 pilot tones (7 CW signals) to boost the input power level entering the EDFA, the BER was improved to 4.11E-5 for OOK modulation and 3.25E-7 for DSPK modulation. No eye diagram was taken at the time of the measurement since the measurements were meant to be repeated with the new hardware (the new EDFA were never purchased due to budget constraints).

The second experiment constituted a proof of concept of the loop's functionality. We have chosen the DPSK modulation, as it had the best BER in the straight line experiment. The signal was circulated twice around the loop and its BER was measured. After 500km of propagation, the measured BER of our signal was 3.4E-3 which is below the FEC error free limit. Our transmission was noise limited from all the ASE generated by the EDFAs.

Our last experiment was intended to measure the gain flatness of the inline EDFAs in a multi-channel setup. We have used 8 available lasers (see section 1.3.2.1) to build a testbed of 8 channels at 10 Gb/s. After one loop length the difference in power between the two extreme channels was of 12.42dB.

There are two main problems with the current inline EDFAs from Optilab. First, the minimal input power per channel needs to be higher than -16dBm. With our current

setup, signals entering the EDFAs are as low as -29dBm. The second problem with the EDFAs is that the gain is not flat for the required input powers so the relative power difference between channels diverges quickly with each turn around the loop (Figure 28). After each EDFA, the lower signal wavelengths will receive a higher gain than the higher signal wavelengths. These amplified signals, after propagation in the optical fiber, will serve as input for the next EDFA. Since all EDFAs have the same gain profile, the effect is cumulative. For an input signal with O.2dB power variation across the channels, the output signal had a 4.17dB power variation after 1 EDFA and 12.42dB after one full loop. The purchased amplifiers had fixed output power (minimum 18dBm) and were overdriving the gain for channel profiles of maximum 16 channels available in the lab; as such, the output profile was always tilted. There are two possible solutions for this issue.

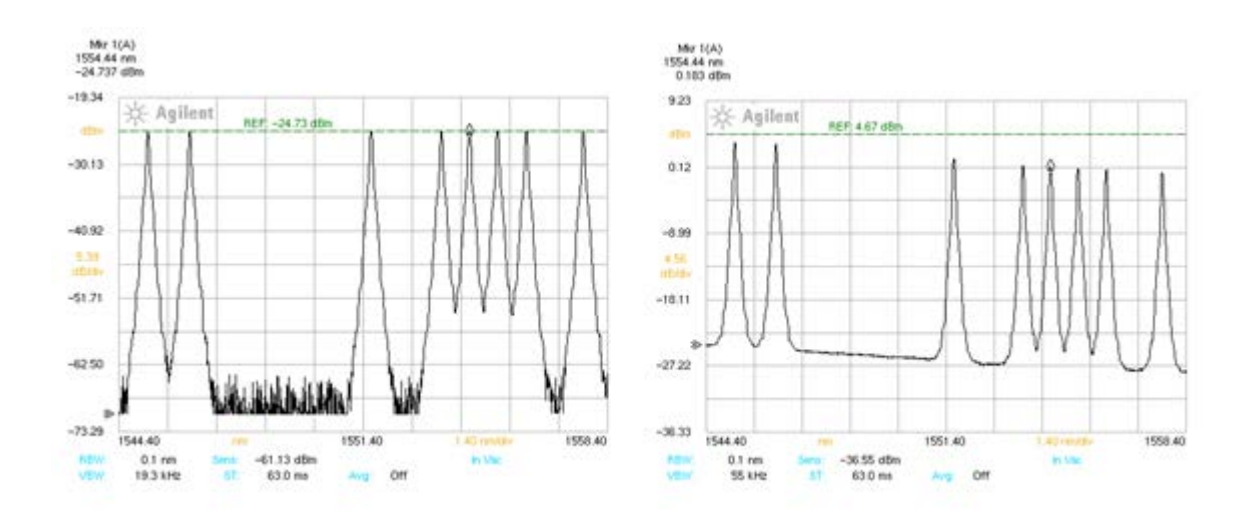


Figure 28 Gain flatness of Optilab's inline EDFAs: input signals of -15.7dBm total power (left), output signals of 10.1dBm (right).

Solution 1

This solution involves redesigning the loop length to match the optimal EDFA input power such that the amplifier gain is flat in the frequency range of the signals and NF is minimal. In order to make the current version of the loop functional, the total length per

span needs to be decreased from 80 km to 40 km, which is possible with the current inlab fiber. As such, the power entering the EDFAs will be at a high enough level so that the output is flat and the NF is the lowest possible for these EDFAs (which is specified at 6dB).

Some drawbacks of this solution are: The max distance of the loop will be halved, VOAs are needed after each EDFA to lower to power per channel to the desired level, and the NF is worse compared to an EDFA that amplifies to the needed level, and impossible to predict beforehand.

Solution 2

Three new Oclaro EDFAs need to be purchased. These new EDFAs have variable gain, accept low power per channel levels (-29dBm) and have a flat gain across the C band. The maximum output power of these EDFAs is 18dBm (Please see Appendix for the new inline EDFA). With solution 2 we have: Higher flexibility from variable gain, lower noise figure, higher length per span because of lower input power per channel, but higher cost compared to solution 1.

1.6 Conclusion

In the first part of the thesis, the design of an optical recirculating loop has been demonstrated. After the analysis of different recirculating loops found in the literature, a final architecture was proposed as design for our loop. This final design supported all the features required from this optical testbed: the system supports 16 channels at 40 Gb/s on a 50GHz channel spacing on the ITU grid. The testbed was designed with a lot of flexibility, such that it can accommodate a variety of different experiments employing different fiber types, different dispersion compensating maps and different transmission lengths and different modulation formats. In the last chapter of this section, we showed simulation results that demonstrate the loop's usability for a 16 channel NRZ DPSK and

NRZ QPSK on 50GHz channel spacing for a total of two loop lengths. The longest transmission length was achieved with the RZ-DPSK modulation on 100GHz channel spacing and the total length was 1800km.

Disclaimer: The limited experimental results were due to the unavailability of the equipment (i.e. the purchased amplifiers were grossly out of spec) at the time of the submission of the thesis. The simulation results helped sustain the proposed architecture, however, additional experimental tests are required for the testbed validation.

1.7 References

- [1] E. Pincemin, A. Tana, A. Bezarda, A. Tonellob, S. Wabnitzb, J. D. Ania-Castañónc, S.K. Turitsync, V. Mezentsevc, "Advanced modulation formats for the next generation of 40 Gb/s, WDM terrestrial all-optical European fiber networks", Proceedings of the Symposium on Photonics Technologies for 7th Framework Program, 2006
- [2] G.P. "Agrawal, Lightwave Technology Telecommunication Systems", 2005
- [3] SHF Communication Technologies AG, "Tutorial Note 5 Modulation Schemes"
- [4] E. Pincemin, A. Tan, A. Bezard, A. Tonello, S. Wabnitz, J. D. Ania-Castañón, S.K. Turitsync,
- V. Mezentsev, Advanced modulation formats for the next generation of 40 Gb/s, WDM terrestrial all-optical European fiber networks, Proceedings of the Symposium on Photonics Technologies, 2006
- [5] C. Mamyshev, C. Rassmussen, B. Mikkelsen, "40 Gb/s Upgradability of 10Gb/s systems", IEEE Lasers and Electro-Optics Society (LEOS), pp. 23-24, 2004
- [6] I. Lyubomirsky, "White Paper Advanced Modulation Formats for Ultra-Dense Wavelength Division Multiplexing", University of California
- [7] S. Tsukamoto, D. Ly-Gagnon, K. Katoh, K.Kikuchi, "Coherent Demodulation of 40-Gbit/s Polarization-Multiplexed QPSK Signals with 16-GHz Spacing after 200-km Transmission", IEEE Optical Fiber Communications (OFC/NFOEC), Vol. 6, pp. 3, 2005
- [8] A. H. Gnauck, G. Raybon, S. Chandrasekhar, J. Leuthold, C. Doerr, L. Stulz, E. Burrows, "25 x 40-Gb/s Copolarized DPSK Transmission Over 12 x 100-km NZDF With 50-GHz Channel Spacing", IEEE Photonics Technology Letters, Vol. 15, No. 3, pp. 467-469, 2003
- [9] G. Gnanagurunathan, F. A. Rahman, "Comparing FBG and DCF as dispersion compensators in the long haul narrowband WDM systems", IEEE International Federation for Information Processing (IFIP), pp. 4, 2006
- [10] L. K. Wickham, R.-J. Essiambre, A. H. Gnauck, P. J. Winzer, A. R. Chraplyvy, "Bit Pattern Length Dependence of Intrachannel Nonlinearities in Pseudolinear Transmission", IEEE Photonics Technology Letters, Vol. 16, No. 6, pp. 1591-1593, 2004

- [11] F. Audet, Dispension, "Dispersion Compensating Fiber: Precision and Repetition", ExFO technical note
- [12] D. Z. Chen, T. J. Xia, G. Wellbrock, P. Mamyshev, S. Penticost, G. Grosso, A. Puc, P. Perrier, H. Fevrier, "New Field Trial Distance Record of 3040 km on Wide Reach WDM With 10 and 40 Gb/s Transmission Including OC-768 Traffic Without Regeneration", IEEE Journal of Lightwave Technology, Vol. 25, No. 1, pp. 28-37, 2007
- [13] S. Baruh, M. R. X. de Barros, M. de L. Rocha, M. R. Horiuchi, J. B. Rosolem, R. Arradi, S. M. Rossi, A. Paradisi, M. T. M. Rocco Giraldi and M. A. G. Martinez, "Experimental Demonstration and Numerical Simulation of an Optical Recirculating Loop Operating at 10 Gb/s", IEEE Microwave and Optoelectronics Conference, Vol. 1, pp 239-243, 2003
- [14] Y. Sun, I. T. Lima, Jr., H. Jiao, J. Wen, H. Xu, H. Ereifej, G. M. Carter, C. R. Menyuk, "Study of System Performance in a 107-km Dispersion-Managed Recirculating Loop Due to Polarization Effects", IEEE Photonics Technology Letters, Vol. 13, No. 9, pp. 966-968, 2001
- [15] S. Chandrasekhar, C. R. Doerr, L. L. Buhl, "Demonstration of 100% Precompensated DWDM Transmission Over 1280 km of SSMF With No Inline Dispersion Compensation Using Interconnected Recirculating Loops", IEEE Photonics Technology Letters, Vol. 18, No. 1, pp. 256-258, 2006
- [16] H. Xu, H. Jiao, L. Yan, . Gary M. Carter, "Measurement of Distributions of Differential Group Delay in a Recirculating Loop With and Without Loop-Synchronous Scrambling", IEEE Photonics Technology Letters, Vol. 16, No. 7, pp. 1691-1693, 2004
- [17] M. Petersson, C. Vinegoni, H. Sunnerud, M. Karlsson, "Statistics of PMD in Recirculating Loops", IEEE Photonics Technology Letters, Vol. 15, No. 11, pp. 1543-1545, 2003
- [18] C. Vinegoni, M. Karlsson, M. Petersson, H. Sunnerud, "The Statistics of Polarization-Dependent Loss in a Recirculating Loop", IEEE Journal of Lightwave Technology, Vol. 22, No. 4, pp. 968-976, 2004
- [19] Y.K. Lize, C. Malouin, N. Godbout, S. Lacroix, "Periodic power oscillations from combined effect of polarisation-dependent loss and polarisation evolution in recirculating loops", IEEE Electronics Letters, Vol. 41, No. 3, pp. 148-149, 2005
- [20] H.J. Thiele, A.D. Ellis, I.D. Phillips, "Recirculating loop demonstration of 40Gbt/s alloptical 3R data regeneration using a semiconductor nonlinear interferometer", IEEE Electronics Letters, Vol. 35, No. 3, pp. 230-231, 1999

- [21] G. Raybon, P. J. Winzer, C. R. Doerr, "1-Tb/s (10×107 Gb/s) Electronically Multiplexed Optical Signal Generation and WDM Transmission", IEEE Journal of Lightwave Technology, Vol. 25, No. 1, pp. 233-238, 2007
- [22] A. H. Gnauck, P. J. Winzer, S. Chandrasekhar, "Hybrid 10/40-G Transmission on a 50-GHzGrid Through 2800 km of SSMF and Seven Optical Add—Drops", IEEE Photonics Technology Letters, Vol. 17, No. 10, pp. 2203-2205, 2005
- [23] G. Charlet, E. Corbel, J. Lazaro, A. Klekamp, W. Idler, R. Dischler, S. Bigo, P. Tran, T. Lopez, H. Mardoyan, A. Konczykowska, J.-P. Thierry, "Comparison of system performance at 50, 62.5 and 100 GHz channel spacing over transoceanic distances at 40 Gb/s channel rate using RZ-DPSK", IEEE Electronics Letters, Vol. 41, No. 3, pp. 145-146, 2005
- [24] Y. Su, G.Raybon, Z. Zheng, S. Chandrasekhar, R.Ryf, L. Moller, "40-Gb/s RZ Signal Transmission in a Transparent Network Based on Wavelength-Selective Optical Cross Connect", IEEE Photonics Technology Letters, Vol. 15, No. 10, pp. 1467-1469, 2003
- [25] T. Kawanishi, T. Sakamoto, M. Izutsu, "High-Speed Control of Lightwave Amplitude, Phase, and Frequency by Use of Electrooptic Effect", IEEE Journal of Selected Topics in Quantum Electronics, Vol. 13, No. 1, pp. 79-91, 2007
- [26] A. H. Gnauck, G. Charlet, P. Tran, P. J. Winzer, C. R. Doerr, J. C. Centanni, E. C. Burrows, T. Kawanishi, T. Sakamoto, and K. Higuma, "25.6-Tb/s WDM Transmission of Polarization-Multiplexed RZ-DQPSK Signals", IEEE Journal of Lightwave Technology, Vol. 26, No. 1, pp. 79-84, 2008
- [27] N. Yoshikane, I. Morita, "1.14 b/s/Hz Spectrally Efficient 50 85.4-Gb/s Transmission Over 300 km Using Copolarized RZ-DQPSK Signals", IEEE Journal of Lightwave Technology, Vol. 23, No. 1, pp. 108-114, 2005
- [28] Djafar K. Mynabaev and Lowell L. Scheiner, "Fiber-Optic Communications Technology", Prentice Hall, 2001
- [29] E. Desurvire, J. Simpson, and P.C. Becker, "High-gain erbium-doped traveling-wave fiber amplifier", Optics Letters, vol. 12, No. 11, pp. 888-890, 1987
- [30] Cisco Systems, "Understanding Long-Haul Optical Networks", 2003
- [31] Fiber Optics Technology, "Optical Amplifiers", online reference: http://www.fiber-optics.info

- [32] M. Funabashi, "Demonstration of Optical 3R Regenerator for 10 Gb/s NRZ signal in Reconfigurable Recirculating Loop Transmission", IEEE Photonics International Conference on Photonics in Switching, pp. 1-3, 2006
- [33] S. Baruh, "Experimental Demonstration and Numerical Simulation of an Optical Recirculating Loop Operating at 10 Gb/s", Proceedings SBMOI IEEE, 2003
- [34] S. Weisser, "Single-Channel 170Gb/s Transmission up to 4000km using Dispersion-Managed Fiber Spans and all-Raman Amplification", IEEE 31st European Conference on Optical Communication (ECOC), Vol. 3, pp. 439-440, 2005
- [35] Y. Sun, "Variation of system performance in a 107 km dispersion managed recirculating loop due to polarization effects", IEEE Conference on Lasers and Electro-Optics (CLEO), pp. 566-567, 2001
- [36] Telecommunication Standardization Sector of ITU, "Transmission media characteristics Optical fibre cables", ITU-T G.652.D, 2005
- [37] B. Chomycz, "Planning Fiber Optic Networks", Mc-Graw Hill 2009
- [38] T. Breach, "40Gbps and plus", NORDUnet, White Paper
- [39] G.P. Agrawal, "Lightwave Technology -- Telecommunications Systems", Chapter 8 Nonlinearity Management, p. 287
- [40] M. Zaacks, U. Mahlab, "1000 km 43 Gbps RZ-DPSK Transmission Through a 50 GHz Channel Spaced WSS", IEEE Optical Fiber Communication (OFC), pp. 1-4, 2007
- [41] ECI Telecom, "40G Transmission in Metro and Long-Haul Networks", White Paper
- [42] J. Renaudier, "Transmission of 100Gb/s Coherent PDM-QPSK over 16x100km of Standard Fiber with allerbium amplifiers", Optics Express, Vol. 17, No. 7, pp. 5112-5119, 2009

2 Analysis and Reduction of Polarization Dependent Penalty in Phase Shift Keying Demodulators

2.1 Background Theoretical Review

Applications such as video and high-speed Internet are responsible for the tremendous traffic growth on the optical transport network. Moreover, the deployment of fiber-tothe-home with higher data rates is putting pressure on Internet Service Providers to upgrade to the next-generation optical networks. In metro networks, differential phase shift keying (DPSK) is arguably becoming a format of choice due to its more relaxed optical signal to noise ratio (OSNR) margin and greater tolerance to nonlinear effects, which are particularly important at higher data rates [1]. An optical DPSK-modulated carrier can be demodulated using a Mach-Zehnder delay interferometer (DI) with a one additional bit delay in one arm relative to the other arm, such that the phase in one time slot interferes with the differentially encoded successive time slot [2]. The introduction of the relative bit delay changes the filtering function of the Mach-Zehnder from an all pass to a comb filter characterized by a free spectral range (FSR) determined by the delay, typically chosen to equal the bit period. The frequency response of the DI is usually called transmissivity and is characterized by peaks separated by one FSR. To reduce the filtering effect, the wavelength of the optical carrier is aligned with one of the DI's transmissivity peak. Indeed, a frequency offset between the laser and the DI's transmissivity peak degrades the performance of DPSK optical communication systems as some of the signal power is being asymmetrically filtered, generating a distorted spectrum profile. The penalty was demonstrated to be 1 dB for a 4-5 % frequency offset [3, 4]. A similar worsening effect is caused by the polarization dependence of the DI's effective refractive index, resulting in what is referred to as polarization dependent frequency shift (PDf). Indeed, the shift in the frequency of the filtering function causes a

misalignment between the transmissivity peak and the laser source wavelength of the carrier [2, 4].

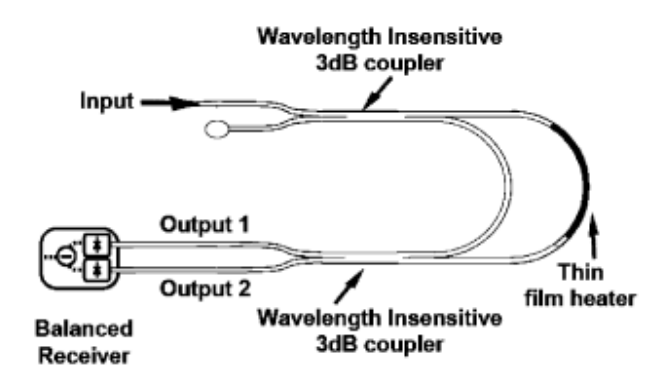


Figure 29: Schematic of the fiber-based DPSK demodulator by ITF Labs/Avensys.

The polarization dependence of the effective refractive index is caused by mainly two factors in the DI's structure shown in Figure 29: (1) the additional birefringence in the fiber bending due to the photoelastic effect, and (2) the polarization crosstalk occurring in the optical couplers of the demodulator causing polarization mode coupling [5, 6]. The birefringence and polarization crosstalk are jointly responsible for a polarization-induced random phase difference ($\Delta \Phi$) between the two arms of the DI. The PDf is the maximum frequency shift, Δf , induced by two orthogonal state of polarization (SOP) of the optical signal. The PDf is defined as $\Delta \Phi / 2\pi * FSR$ for a given interferometer [2]. Hence, the PDf scales linearly with FSR which means that a demodulator for higher data rates will have greater PDf.

There has been some work in reducing the PDf in Mach-Zehnder DIs. Mizuno *et al.* use a Jones Matrix Eigen analysis to model the PDf of a Mach-Zehnder Interferometer (MZI) and demonstrated that the PDf of a MZI can be eliminated by proper adjustment of the arm length [7]. The birefringence of the MZI can also be controlled by inserting stressapplying amorphous silicon film in the waveguide [8]. By laser-trimming these films, the

authors were able to accurately control the birefringence and phase states. In another experiment, Nasu *et al.* recently demonstrated that PDf can be eliminated by the asymmetrical addition of a half wave plate [9]. With the addition of a half-wave plate in both arms of the DI, the authors were able to greatly reduce the DI's PDf penalties incurred from birefringence effects, as well as polarization crosstalk that was occurring in the couplers. A free-space DI design approach can also be used to obtain very low polarization dependent loss (PDL) and PDf [10].

In this part, we first introduce a methodology to efficiently extract the PDf-induced biterror-rate (BER) penalty from the PDL exhibited mainly from the couplers and connectors. While PDf increases with data rates, we show that it is the PDf ratio, defined as PDf/FSR that plays a predominant role in determining the performance of the demodulator for different data rates. We will explain the reasons why this is the case. We also show and explain the optical filtering effect on pulse carving such as 40-Gb/s Return-to-Zero (RZ) DPSK modulation formats. An additional 0.3 dB penalty compared to Non-Return-to-Zero (NRZ) was measured due to PDf alone. Finally, a cost effective technique to reduce the PDf induced BER penalty is presented and validated. The PDf penalty is further mitigated by 40 % using a PDL emulator to add losses in one of the polarization axes.

2.2 PDf Performance Penalty Analysis

2.2.1 Measurement Methodology

The PDf of a delay interferometer (DI) is conventionally assessed by measuring the optical output power across the optical bandwidth of the DI for different state of polarization (SOP) of the optical signal at the input. A shift in the transmissivity peak will occur, corresponding to the PDf. This approach requires a tunable laser and does not necessarily give accurate measurements as other polarization effects (e.g., polarization

dependent loss), is not explicitly removed from the measurement. The measurement methodology introduced in this section requires only one fixed laser and removes PDL contributing penalties.

In commercial DIs (

Figure 29), a thin film heater is directly deposited on the optical fiber to control the phase of the DI. This way, the FSR can be thermally shifted by applying a voltage across the thin film heater. The frequency shift of the FSR profile is linearly proportional to the applied voltage. Hence, the peak of transmissivity can be maximized for different SOP of the input optical signal by thermo-electrically compensating the optical power degradation due to the inherent polarization dependence of the DI. The measurements are repeated for several SOP settings uniformly covering the Poincaré sphere to determine the maximum frequency shift possible (Figure 30).

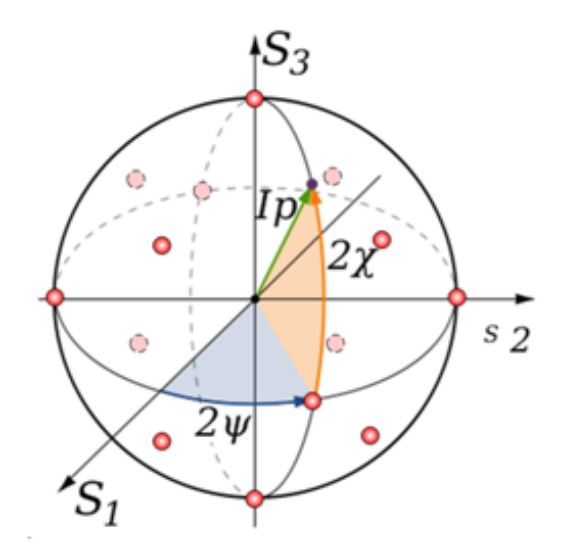


Figure 30 The Poincare Sphere showing the 14 SOP that were chosen for these experiments [12]

The SOP of the optical signal is set using a polarization controller at the input of the demodulator. Once the maximum frequency shift of the FSR is determined, PDL inherent to the demodulator is quantified from the difference in the power of the two

transmissivity peaks. The two SOPs of the input optical signal corresponding to the maximum shift in the FSR are orthogonal and represent the fast and slow polarization axis of the demodulator.

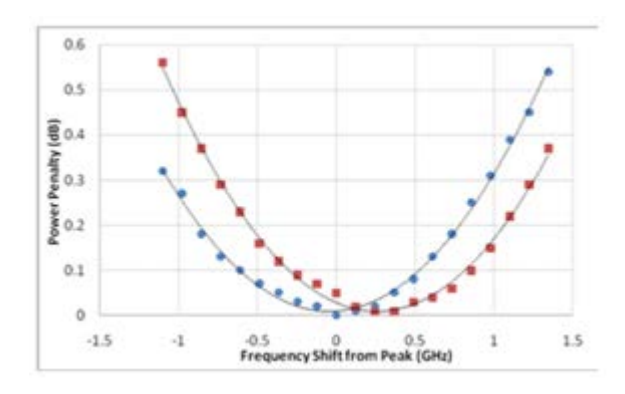


Figure 31: Power penalty versus frequency shift for two orthogonal SOPs of a 10-Gb/s demodulator.

Following the methodology described above, the measurements of a 12-GHz demodulator for 10-Gb/s optical systems were taken (Figure 31). For the frequency shift increments, the voltage source limited it to 50 MHz. The measured PDf is 350 MHz which is comparable to the reported PDf by the manufacturer of 360 MHz, measured using Jones Matrix Eigen analysis (JME). The measurements were fitted to the profile of the Dl's transmissivity and the curve equation was found to be $\sin^2(0.239*f)$, where f corresponds to the frequency shift (x-axis). From this equation, the FSR is then estimated to be 13.11 GHz. For a known FSR, the normalized power penalty caused by PDf can therefore be approximated using the following mathematical relationship $\sin^2(\pi \cdot PDf/FSR)$ [11].

Greater accuracy in measuring small frequency shifts can be obtained using an optical spectrum analyzer with ultra-high resolution (20 MHz). In Figure 32, the optical output signal spectra of both the constructive and the destructive port of the demodulator are observed. Evidently, the frequency shift due to the polarization dependence of the

demodulator is visible on both ports. The optical output signal of the destructive port is used to align the DI's peak transmissivity with the laser frequency for any arbitrary SOP. The measurements were performed at the nulls of the signal spectra where the spectrum exhibits clearer and more abrupt transitions for smaller frequency shift measurements. This methodology was used in the following subsections for greater accuracy.

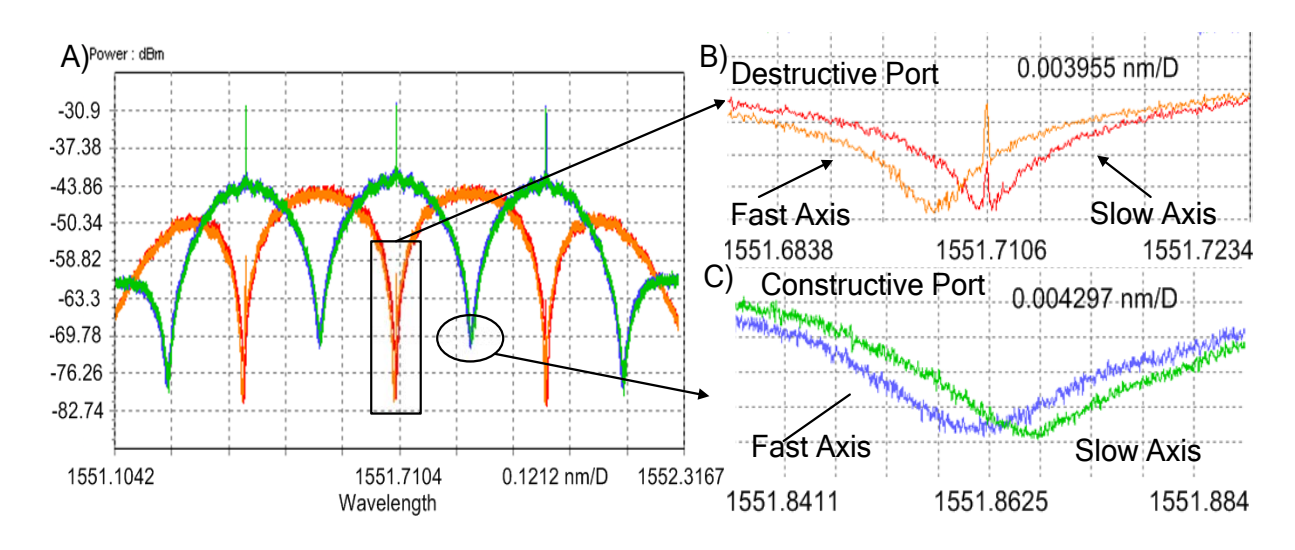


Figure 32: Signal spectra of the demodulator showing both the destructive and constructive ports, with (top) a zoom on a spectral null of the destructive port and (bottom) of the constructive port.

2.2.2 PDf effect versus bit rate

For a given delay interferometer, the PDf increases with FSR. However, the PDf penalty depends not only on the PDf of the DI but also on its FSR. In fact, the PDf ratio (i.e., PDF/FSR), is a key parameter to evaluate the PDf-induced penalty. To explain why this is the case, we illustrate the effect using two demodulators, one with a FSR of 10 GHz, and one with a FSR of 40 GHz. For this example, the PDf for both demodulators is assumed to be 1 GHz. The PDf ratio is therefore 10% and 2.5% for the 10-GHz and 40-

GHz DIs, respectively. In Figure 33, the power cutoff in the spectrum profiles due to a shift is shown. Correspondingly, distortion in the spectrum occurs due to the asymmetrical filtering effect. The power loss can be defined as a function of the total power, corresponding to 38.6% for the 10-GHz DI compared to 10% for the 40-GHz DI. Hence, for the same PDf value, the power loss is four times worst for the DI with a smaller FSR (10 GHz in this comparison), since more portion of the power is being cut off. For this reason, the PDf ratio is a better indicator of the PDf-induced penalty. The PDf ratio is not a new idea and it is used in literature to normalize the PDf of DIs. In [14], the authors use the PDf ratio to compare different DIs' architectures.

We experimentally verified this conclusion using two DIs. A 40-Gb/s demodulator (FSR of 40 GHz, PDf of 600 MHz) is compared with a 10-Gb/s demodulator (FSR of 12 GHz, PDf of 360 MHz). The testbed used is shown in Figure 34 where a single distributed feedback (DFB) laser output (1551.7 nm) is modulated using a Mach-Zehnder modulator (MZM) appropriately biased to create NRZ-DPSK modulated data. The MZM is driven by a pseudorandom bit sequence with a length of 2³¹-1. An erbium doped fiber amplifier (EDFA) is used to compensate the losses of the modulators. The out-of-band noise generated by the amplifier is filtered using a 0.9-nm band pass filter (BPF). A variable optical attenuator (VOA) is used to compensate for small PDL originating from the 95/5 splitter (measured to be 0.3 dB). As mentioned in the previous measurements, the polarization controller (PC) in front of the DI is used to change the SOP of the optical signal entering the DI. In order to track the signal's SOP, we use a polarization analyzer (PA). The optical demodulated signal is then converted to electrical using an optical receiver and analyzed using a bit-error-rate tester (BERT).

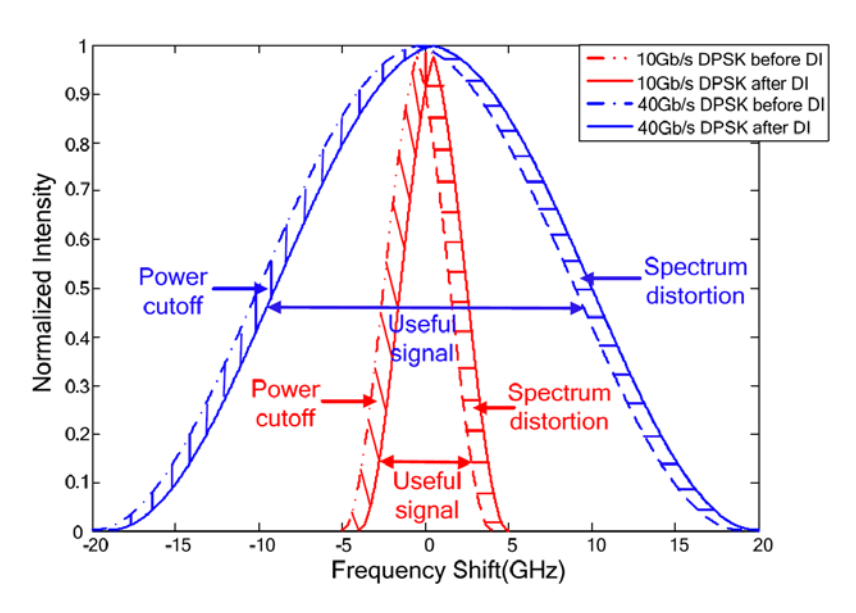


Figure 33: Comparison of the spectrum of a 10-GHz and a 40-GHz DI.

To assess the PDf penalty at different bit rates, the bit-error-rate (BER) is measured for small wavelength changes from the transmissivity peak of the constructive port. The BER is measured for the two orthogonal SOPs corresponding to the slow and fast polarization axis of the 10-Gb/s demodulator and the 40-Gb/s demodulator. The PDf will impose a BER penalty on the signal.

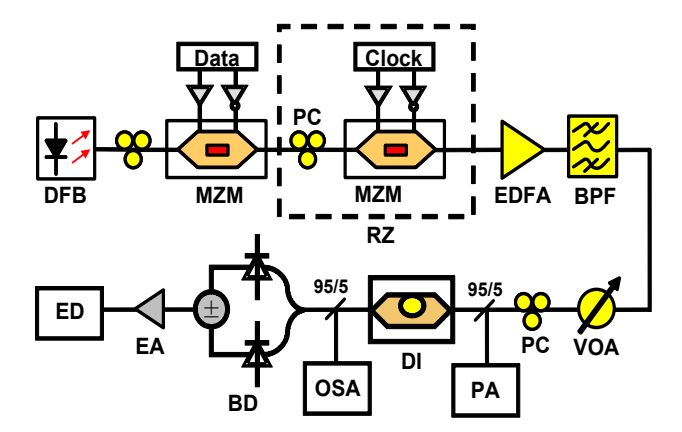


Figure 34: Experimental setup for PDf analysis versus data rate.

In Figure 35, the first observation is that the 10-Gb/s NRZ-DPSK system is more sensitive to frequency misalignments between the laser frequency and the transmissitivity peak. Despite this behavior, the PDf of the 40-GHz DI (600 MHz) is almost the double of the 12-GHz DI one (360 MHz). As shown in the zero-frequency shift point (Figure 35b), the BER penalty of the 12-GHz DI is around 0.90 dB versus 0.12 dB for the 40-GHz DI which is 7.5 times less. The BER penalty used here is defined as 10-log(BER₁/BER₂) where BER₁ and BER₂ correspond to the BER measurements of the two orthogonal axes at zero frequency shift. The penalty differences can be explained by the PDf ratio. The PDf ratio of the 10 GHz DI is 3 % while that of the 40 GHz DI is only 1.5 %. Smaller PDf ratios result in smaller BER penalties. This ratio enables the comparison of DPSK demodulators with different PDf and FSR characteristics.

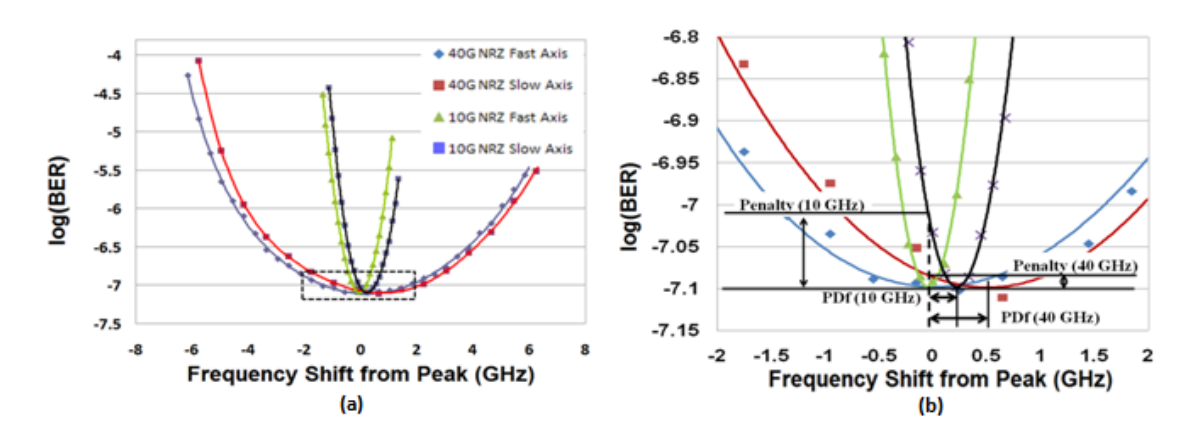


Figure 35: BER versus frequency detuning. (a) All measurements shown. (b) Zoom in dotted rectangle PDf and penalty for the respective DIs.

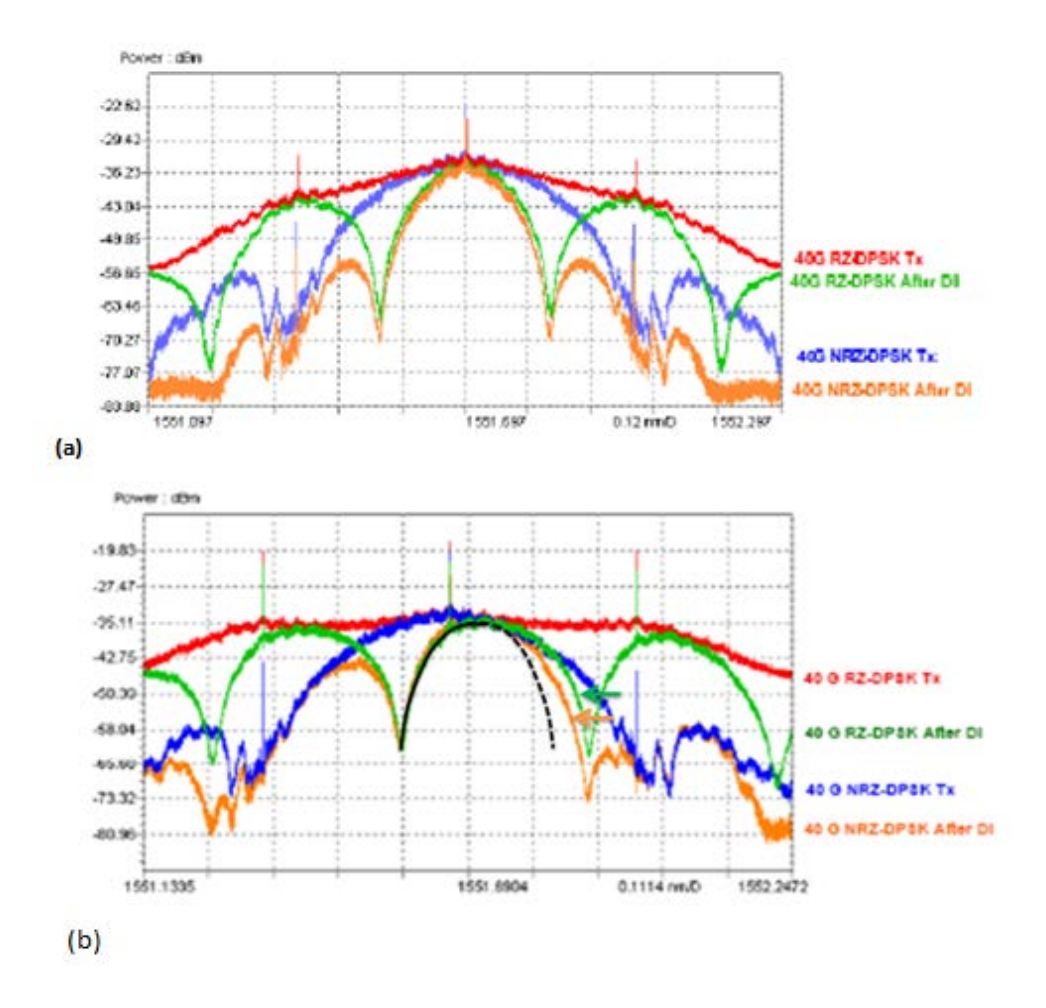


Figure 36: (a) Spectra of 40-Gb/s NRZ- and RZ-DPSK signals (b) showing the effect of frequency offset.

2.2.3 PDf versus pulse carving

At higher data rates, pulse carving is used to alleviate some of the dispersion effects. In such context, the PDf-induced penalty was further analyzed to compare the demodulation of 40 Gb/s NRZ-DPSK signals and 40 Gb/s RZ-DPSK signals to study the effect of smaller FSR compared to the bandwidth of the signal. Indeed, RZ modulation exhibits a spectrum width that is almost doubled compared to NRZ-DPSK. Consequently, RZ demodulated signals have more residual optical power in the adjacent spectrum lobes compared to NRZ, which has most of its power in the main lobe. Intuitively, the RZ

signal should suffer from additional optical filtering imposed by the FSR of DI. If the demodulator is perfectly aligned with the DI, the spectral filtering will be symmetrical and the demodulated signal will keep its symmetry. Any small variations of the alignment will break this symmetry incurring spectrum distortion (Figure 37). As a result, RZ-DPSK signal is less tolerant to PDf. The experimental spectra shown in Figure 36 illustrate the effect of a deliberately large frequency offset (11.4 GHz) with respect to the transmissivity peak. It can be seen that RZ-DPSK suffers more from the power filtering resulting from greater asymmetry and consequently spectral distortion.

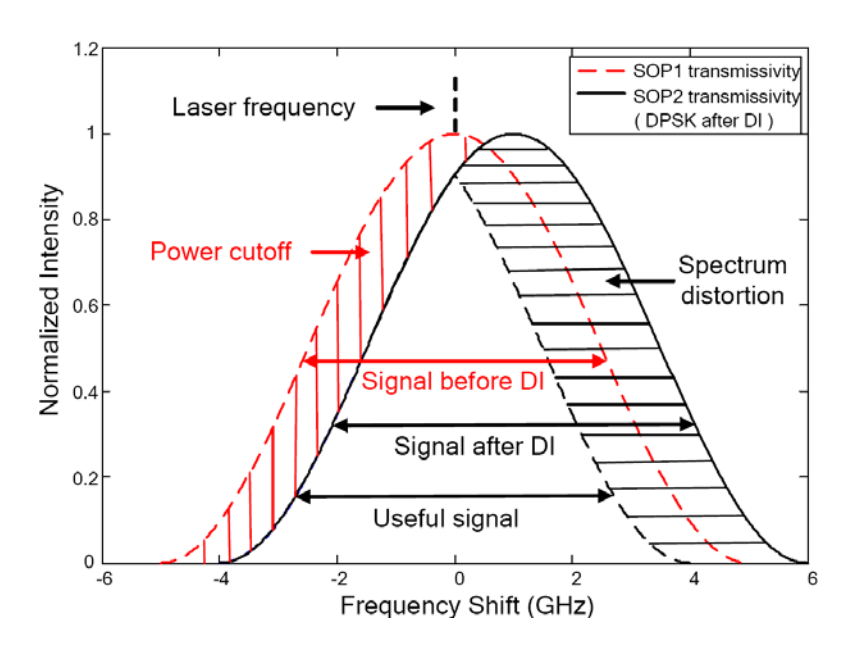


Figure 37: Spectral profile of a RZ-DPSK signal

To experimentally measure the associated PDf-induced penalty due to pulse carving, the minimal BER was set to be the same for both NRZ and RZ. This implies that in the case of RZ pulses, the required OSNR to achieve the same BER is greater to account for the power loss from optical filtering. An additional MZM (shown in the dashed square in Figure 34) is used to carve the pulses at 50 % using the 40 GHz clock for the cases of RZ-DPSK modulated signals. Figure 36b shows the comparison of BER penalty between a 40 Gb/s RZ-DPSK and a 40 Gb/s NRZ-DPSK signal. As it can be seen, RZ pulses are more

sensitive to frequency shifts. The measured PDf induced BER penalty for the 40-Gb/s NRZ signal was measured to be 0.12 dB compared to 0.46 dB for the 40-Gb/s RZ signal.

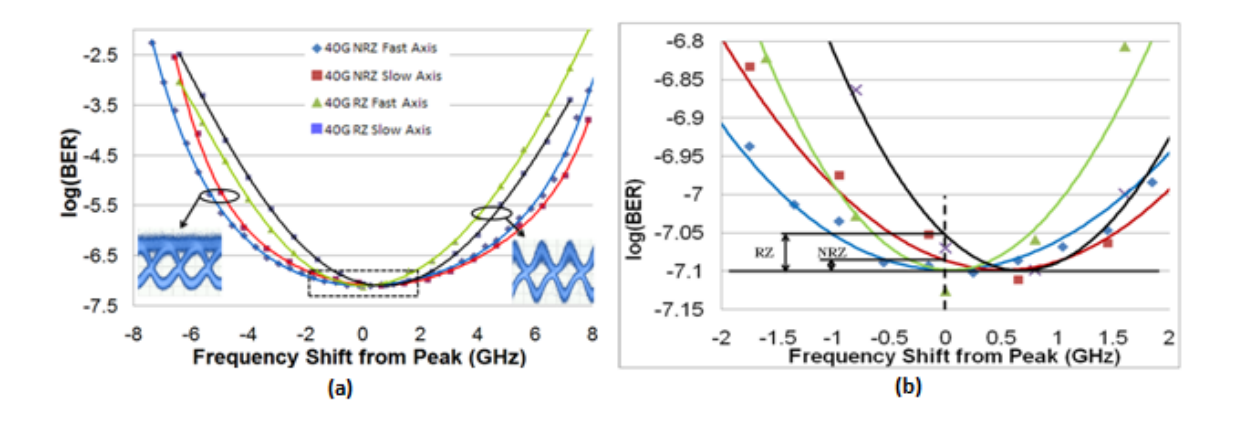


Figure 38: BER versus frequency detuning for demodulated 40 Gb/s RZ- and NRZ- DPSK signals: a) all measurements, b) zoom closer to transmissivity peak.

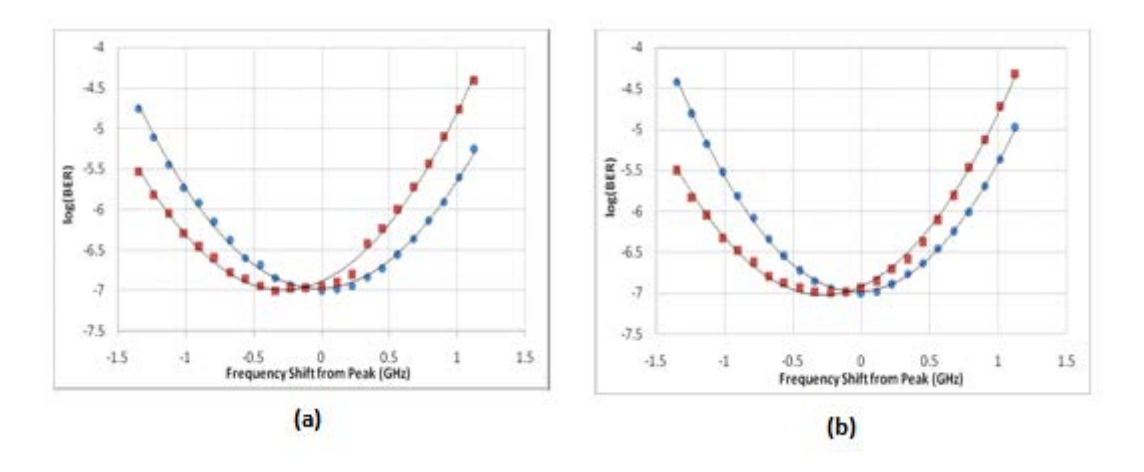


Figure 39: (a) BER penalty vs. frequency shift of the slow (red dots) and fast (blue dots) polarization axis of a 10 Gb/s demodulator. (b) Reduced PDf with calibration. (The continuous lines in graphs above represent the fitted curves to the dot experimental data on the same graph)

2.3 Mitigating PDf Effect

2.3.1 Cost-effective Solution

A cost-effective way to reduce the PDf-induced penalty can be achieved through proper calibration of thermo-electrically compensated demodulators. After finding the two voltages values that compensate for the slow and fast polarization axis as described in section 2.2.1, the voltage value corresponding to half the difference is applied to the DI. This way, the DI is tuned to maximally demodulate optical signals of any SOP inducing only at most half the frequency shift associated to the PDf [11, 12]. This effective PDf is shown in Figure 39b, which is 188MHz with a BER penalty of 0.46dB for a DI with an device PDf of 375 MHz. The 188MHz and 375MHz values were calculated from the minima of the fitted lines (a zoom-in vizualization of the fitted lines minima is impossible in the figure due to the quasi flatness of the curves at the minima observation levels). Without calibration, the BER penalty can be as high as 1.5dB (Figure 39a). Although the physical PDf remained constant, the maximum frequency shifts is halved to PDf/2 reducing the PDf-induced penalty.

2.3.2 PDL to Compensate PDf

A PDL emulator was used to reduce the DI's sensitivity to polarization. The PDL emulator consists of a device that splits the light into two orthogonal polarizations. With the use of a Variable Optical Attenuator (VOA), one of the two polarizations is attenuated. The two signals are then recombined, thus inducing a PDL effect on the propagating signal. The PDL emulator has two paths, one with loss and one without. Using a polarization controller, the slow axis path (with loss) is aligned with the fast axis of the DI, thus experiencing no PDf-induced penalty. As a result, the orthogonal SOP going through the slow axis path (lossless path) experiences the maximum PDf effect of

the DI, with its corresponding power penalty. Essentially, the PDf is compensated with PDL.

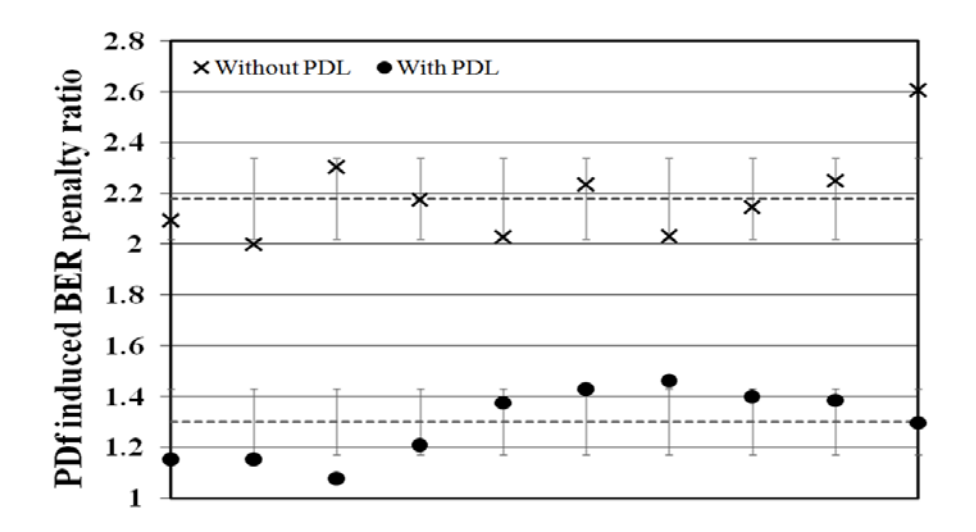


Figure 40: PDf mitigation with BER high and BER low representing the highest and lowest measured BER, respectively, for ten measurements.

To quantify the reduction in polarization sensitivity of the DI, the BER was measured ten times, each for 16 input SOPs spread evenly across the Poincare sphere. The measurement set is repeated twice, once with the PDL emulator and once without it. The highest and lowest BER was measured sequentially. As a figure of merit of the DI's polarization sensitivity, the ratio of the two BER measurements is used. Each measurement was first normalized to the same baseline (i.e. BER of 10^{-7}). The results are presented in Figure 4040 where noticeable improvement can be observed. The calculated 99% confidence interval was calculated using a Taylor series approximation of Fieller's theorem [16]. The DI's sensitivity to polarization was found to be 2.18 \pm 0.16. The ratio dropped to be 1.3 \pm 0.13, a 40 % reduction in sensitivity. The sensitivity to PDf was reduced by 40%. Note that a ratio of 1 corresponding to polarization insensitive could not achieved due predominately to the use of discrete components which

introduced their own polarization-induced BER penalty. We think that the results could be better through device integration.

We can also calculate the improvement in Q-factor due to the addition of the PDL emulator. Using equation 10 [1], we can approximate the Q-factor for a known BER.

$$BER = \frac{1}{2} erfc \left(\frac{Q}{2}\right) \approx \frac{1}{Q\sqrt{2\pi}} e^{\frac{Q^2}{2}}$$
(10)

Figure 41 shows the Q-factor penalty incurred from PDf with and without our PDL emulator. We can see that the/Q-factor penalty function shape resembles the BER-penalty function shown in Figure 40. When no PDL emulator was used the system experienced a Q-penalty of $0.19dB \pm 0.038dB$. With the addition of our PDL emulator, the Q-penalty decreased to $0.06dB \pm 0.048dB$. The Q-factor improvement when using the PDL emulator was 0.13dB.

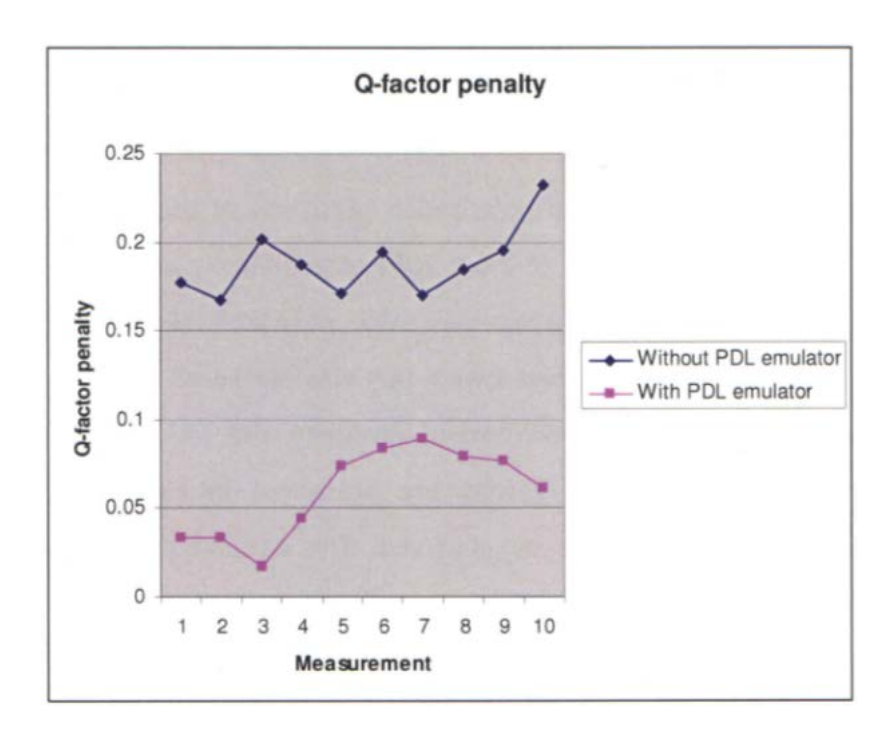


Figure 41 Q-factor penalty due to PDL

2.4 Conclusion

In this part, we have presented a readily available method of measuring the PDf of a delay interferometer (DI) for DPSK demodulation. Using the methodology, the corresponding PDf-induced penalty for 10 and 40 Gb/s NRZ and RZ-DPSK systems was explained and experimentally investigated. We found that the penalty has a large dependence on the PDf ratio rather than PDf alone. We also showed the PDf induced penalty becomes larger in cases where the signal bandwidth is wider than the FSR of the DI. Indeed, RZ modulation experiences additional filtering of its optical power spectrum leading to greater spectrum distortion from asymmetric filtering. The work was concluded with a cost-effective calibration of the DI's phase component on one of the DI's branches to effectively reduce the PDf induced BER penalty by half. Moreover, adding PDL to compensate for PDf is shown to be an effective design to mitigate the DI polarization sensitivity by 40 % and effectively improve the Q-factor by 0.13dB.

The PDL emulator method presented in section 2.3.2 does not completely compensate the PDf induced penalty. There are other methods, such as a device to track the Q factor and adjust the polarization state of the signal to obtain the lowest penalty possible, to more effectively mitigate the PDf induced penalty. However, such methods are more costly and not in line with the DPSK modulation low cost philosophy (a detailed cost / benefit analysis is beyond the scope of this work).

Conclusion and Future Work

The subject matter presented in this thesis follows a general to particular chronological narrative. First, the design and testing of a 40Gb/s optical recirculating loop is presented. Whereas this testbed necessitated an analysis of the various link components' requirements to combat the link impairments and satisfy the system timing and link budget requirements; the second part of the thesis was much more specific and focused on one particular impairment of one particular link component: the analysis and reduction of PDf in phase shift keying demodulators.

The optical design loop will be used in a variety of experiments by other members of the lab when studying advanced modulation techniques. For a more detailed description of the loop's functionality please consult the conclusion in section 1.6. The testbed can be used as such, but the replacement of three amplifiers is strongly encouraged in order to improve performance and usability. This testbed can be further modified by the subsequent users in order to improve the performance and usability of the setup depending on the different needs at a future time, but the changes are likely to be minimal since the most work has already been done. An example of an upgrade to the setup is changing the transmitters and receivers to operate at 100GB/s.

The investigation of the PDf penalty in DPSK demodulators amounted in a cost effective calibration technique allowing the reduction of the BER by half, and also a technique allowing the DI's polarization sensitivity by 40% by introducing a PDL element before the DI. For a more detailed description of the findings please consult the conclusion in section 2.4. Both techniques are useful since they provide insight in the phenomena related to the receiver's polarization characteristics, but most importantly they are also cost effective solutions. Moreover, even though these techniques have been studied in the context of receivers, they can also be applied to other optical link components that employ MZDIs, such as optical filters. In optical filters employing cascades of MZDI, the polarization effects can be significant. As such, it would be

interesting to investigate the application of the two techniques described above in the context of cascaded MZDI optical filters.

2.5 References

- [1] G.P. "Agrawal, Lightwave Technology Telecommunication Systems", 2005
- [2] A,H. Gnauck, P.J. Winzer, "Optical phase-shift-keyed transmission," J. of Lightwave Technology, vol.23, no.1, pp. 115-130, Jan. 2005
- [3] G. Bosco and P. Poggiolini, "The Impact of Receiver Imperfections on the Performance of Optical Direct-Detection DPSK," Journal of Lightwave Technology, vol. 23, pp. 842-8, 2005.
- [4] H. Kim, P. J. Winzer, "Robustness to Laser Frequency Offset in Direct-Detection DPSK and DQPSK Systems", Journal of Lightwave Technology, Vol. 21, No. 9, 2003
- [5] G. Heise, and R. Narevich, "Simple model for polarization sensitivity of silica waveguide Mach-Zehnder interferometer," IEEE Photonic Technology Letters, vol.17, no.10, pp. 2116- 2118, Oct. 2005
- [6] C.R. Doerr, M.A. Cappuzzo, E.Y. Chen, A. Wong-Foy, L.T. Gomez, S.S. Patel, S. Chandrasekhar, A.E. White, "Polarization-insensitive planar lightwave circuit dual-rate Mach-Zehnder delay-interferometer," IEEE Photonic Technology Letters, vol. 18, no. 16, Aug. 2006.
- [7] T. Mizuno, M. Kohtoku, M. Oguma, Y. Hida, Y. Inoue, "Birefringence and path length adjustment of silica-based waveguide using permanent heater trimming", Electronics Letters, Vol. 40, No. 6, 2004.
- [8] Y. Hashizutne, R. Kasahara, T. Saida, Y. Inoue, M. Okano, "Birefringence control of silica waveguides on Si and its application to a polarization-beam splitter/switch,"

 Journal of Lightwave Technology, vol. 12, no. 4, 1994.
- [9] Y. Nasu, M. Oguma, T. Hashimoto, H. Takahashi, Y. Inoue, H. Kawakami, E. Yoshida, "Asymmetric Half-Wave Plate Configuration of PLC Mach-Zehnder Interferometer for Polarization Insensitive DQPSK Demodulator", Journal of Lightwave Technology, Vol. 27, No. 23, 2009.
- [10] A. G. Steffan, M. L. Nielsen, A. Umbach, A. Boutin, L. Fulop, and F. Verluise,

- "Integrated 40 Gb/s DPSK Receiver Module for C+L Band with Athermal Free-Space Delay-Line Interferometer," in Asia Communications and Photonics Conference and Exhibition, Technical Digest (CD) (Optical Society of America, 2009), paper ThW3.
- [11] D. Cotruta, O. Liboiron-Ladouceur, Y. Lize, and D. V. Plant, "Polarization Dependent Power Penalty in DPSK Demodulation", CLEO 2009, JThE78, 2009.
- [12] D. Cotruta, , X. Xu, D. V. Plant, O. Liboiron-Ladouceur, "Polarization Dependent Frequency Shift Induced BER Penalty in DPSK", 22nd Annual Meeting of the IEEE Lasers and Electro-Optics Society (LEOS), 2009.
- [13] Y. Sakamaki, Y. Nasu, T. Hashimoto, K. Hattori, Y. Inoue, H. Takahashi, "Operation Range Enhancement of Silica Waveguide 43 Gbit/s DQPSK Demodulator by Using Stress Release Grooves", 21nd Annual Meeting of the IEEE Lasers and Electro-Optics Society (LEOS), 2008.
- [14] Y. Nasu, Y. Hashizume, Y. Sakamaki, T. Hashimoto, K. Hattori, Y. Inoue, "Reduction of Polarization Dependence of PLC Mach-Zehnder Interferometer Over Wide Wavelength Range", Journal of Lightwave Technology, Vol. 27, No. 21, 2009.
- [15] Y.K. Lize, M. Faucher, E. Jarry, P. Ouellette, E. Villeneuve, A. Wetter, F. Seguin, "Phase-Tunable Low-Loss, S-, C-, and L-Band DPSK and DQPSK Demodulator", IEEE Photonics Technology Letters, Vol. 19, No. 23, 2007.
- [16] E. C. Fieller, "Some problems in interval estimation," Journal of the Royal Statistical Society B 16 (2): 175–185, 1954

Appendix ---- Optical Specs

Laser
Fitel DFB Lasers

Description
1557.36nm CW Laser, 20mW LD Anode
Ground, <2MHz Linewidth
1556.96nm CW Laser, 20mW LD Anode
Ground, <2MHz Linewidth
1556.55nm CW Laser, 20mW LD Anode
Ground, <2MHz Linewidth
1555.75nm CW Laser, 20mW LD Anode
Ground, <2MHz Linewidth
1554.94nm CW Laser, 20mW LD Anode
Ground, <2MHz Linewidth
1553.33nm CW Laser, 20mW LD Anode
Ground, <2MHz Linewidth
1552.93nm CW Laser, 20mW LD Anode
Ground, <2MHz Linewidth
1552.52nm CW Laser, 20mW LD Anode
Ground, <2MHz Linewidth
1551.12nm CW Laser, 20mW LD Anode
Ground, <2MHz Linewidth

AWG Enablence

Parameter	Symbol	:	Specification			Comments
		MIN	ТҮР	MAX		
Channels	-		40		-	
Channel Spacing	-		50		GHz	
Channel Frequency	f _c	19	94.40 to 192.	THz	Corresponds to 1542.142 to 1557.768nm	
Wavelength Accuracy	Δf _c	-0.03		+0.03	nm	Offset from ITU grid
ITU Band	РВ	-5		+5	GHz	Centered at each ITU frequency
Insertion Loss	IL			6.0	dB	Maximum with ITU band
Insertion Loss Uniformity	ΔIL			1.5	dB	Overall channels
Polarization Dependent Loss	PDL			0.5	dB	Maximum with ITU band
1dB Passband	Δ1dB	0.18			nm	Measure 1dB down from min IL at average

					polarization
3db	δ3dB	0.28		nm	Measure
Passband					3dB down
					from min IL
					at average
					polarization
Adjacent	AX	22		dB	Minimum
Channel					with ITU
Isolation					band
Non-	NX	30		dB	Minimum
adjacent					with ITU
Channel					band
Isolation					
Total	TX	19		dB	Cumulative
Isolation					sum of all
					AX and NX
Return Loss	RL	45		dB	May depend
					on
					connector
					style

Mach-Zehnder modulator

Avanex

Parameters	Specification	Units
Operating Wavelength Range	1525 – 1615	nm
Insertion Loss	<6	dB
Optical Return Loss	>45	dB
Extinction Ratio	>20	dB

RF amplifier

SHF

Parameter	Symbol	Unit		Specification		Conditions
			MIN	TYP	MAX	
High frequency 3dB point	f _{HIGH}	GHz	41			
Low frequency 3dB point	f _{LOW}	GHz			36	
Gain	G	dB	27	30		Inverting
Gain control function		V	0		-5	Reduces gain by
		mA	0		10	more than 3dB
Output power at 1dB compression	P _{01dB}	dBm (V)		24		
Output power at saturation	P _{sat}	dBm (V)		29		
Maximum input power		dBm		4		In operation
				10		Without power supply

Booster EDFA Optilab

Parameter	Specification			Unit
	MIN	ТҮР	MAX	
Maximal Output power	18		23	dBm
Input Signal Level	-2			dBm
Number of channels			42	-
Gain Flatness		1		dB
Noise Figure		6		dB

Inline EDFA

Oclaro

Parameter	Specification			Unit
	MIN	TYP	MAX	
Wavelength Range	1529		1564	nm
Input Power	-27		1	dBm
Gain	17		29	dB
Mid-stage Loss			7.5	dB
Output Power			18	dB
Gain Flatness		0.7	1.3	dB

Noise Figure	5.5	6.1	dB
Polarization Dependent Gain		0.5	dB
Polarization Mode Dispersion		0.3	ps

Optilab

Parameter	Specification			Unit
	MIN	TYP	MAX	
Wavelength Range	1528		1564	Nm
Output Power	15		23	dBm
Input Power	-14		6	dBm
Gain	10		23	dB
Mid-stage Loss			8	dB
Gain Flatness			1	dB
Noise Figure			5.2	dB
Polarization Dependent Gain			0.2	dB
Polarization Mode Dispersion			0.5	ps

Pre-Amplifier EDFA Optilab

Parameter	S		Parameter Specification		Unit
	MIN	TYP	MAX		
Wavelength Range	1528		1564	Nm	
Output Power		Variable		dBm	
Input Power	-29			dBm	
Gain			25	dB	
Noise Figure			4.5	dB	
Polarization Dependent Gain			0.2	dB	
Polarization Mode Dispersion			0.5	ps	

Acousto-Optical Modulator Gooch & Housego

Parameter	Specification	Unit
Acoustic Mode	Longitudinal	-
Wavelength Range	1300-1600	nm
Static Transmission	>97	%
Operating Frequency	35	MHz
Diffraction Efficiency	>85	%
Light Polarization	Random	-
Optical Power Density	<50	KW/cm²
Acoustic Aperture Size	2	Mm
Rise Time	260	ns/mm Beam Diamete
Deflection Angle@1550nm	20.6	rad
RF Power Level	<0.5	W
Impedance	50	Ω
VSWR@35MHz	1.2:1	-

Optical fibers

LEAF

Corning

Parameter	Specification			Unit
	MIN	TYP	MAX	
Attenuation (without connectors)			0.22	dB/km
Dispersion	4.5		11.2	ps/(nm*km)
Polarization Mode Dispersion		0.04	0.1	ps/Vkm

SMFe

Corning

Parameter	Specification			Unit
	MIN	ТҮР	MAX	
Attenuation (without connectors)			0.18	dB/km
Dispersion			18	ps/(nm*km)
Polarization Mode Dispersion		0.04	0.1	ps/Vkm

Old SMF

Corning

Parameter	Specification (measured)	Unit	
Attenuation (with connectors)	0.3	dB/km	
Dispersion	17	ps/(nm*km)	
Polarization Mode Dispersion	Not Available	ps/Vkm	

Dispersion Compensation Inline DCF

Parameter	Specification (measured)	Unit
Attenuation (with connectors)	6	dB
Dispersion	-1350	ps/nm
Polarization Mode Dispersion	Not Available	ps/Vkm

DCM

Teraxion

Parameter	Specification			Unit
	MIN	TYP	MAX	
Dispersion			700	ps/nm
Bandwidth	50			GHz
Channel Grid		50		GHz
Dispersion resolution			10	ps/nm
Phase ripple std. dev.			0.08	Rad
Insertion Loss			6	dB
Polarization Dependent Loss			0.3	dB
Polarization Mode Dispersion			0.5	Ps
Input power			27	dBm

Demodulator

ITF Labs

Parameter	Specification	Unit
Free Spectral Range	40	GHz
Isolation	28	dB
PDF	0.55	GHz

Wavelength Range	1530 – 1610	Nm
Differential Delay between Pigtails	<0.25	ps

Photodetector

SHF

Parameter	Specification			Unit
	MIN	TYP	MAX	
Wavelength Range	C	and L ban	d	-
High Frequency 3dB Point	30			GHz
High Frequency 3dB Point			30	kHz
Conversion Gain	350	450		mV/mW
Receiver Sensitivity		-9		dBm
Output Saturation Voltage (peak-peak)		5	6	V
Rise/Fall Times		9	10	ps
Optical Input Power			13	dBm

Clock Recovery SHF

Parameter	Specification			Unit
Data Input				
Bit Rate VCO1	39.8		41.6	Gbps
Bit Rate VCO2	41.6		43.1	Gbps
Input Voltage	50		800	mV
Return Loss		8		dB
Reference Clock Input			1	
Input Frequency	0.622		0.674	GHz
(Bit Rate / 64 mode)				
Input Frequency	1.244		1.348	GHz
(Bit Rate / 64 mode)				
Input Frequency	2.488		2.696	GHz
(Bit Rate / 64 mode)				
Input Voltage	400		800	mV_{pp}